



1 The Monash Simple Climate Model 2 Experiments (MSCM-DB v1.0): An 3 interactive database of mean climate, 4 climate change and scenario 5 simulations

6 By Dietmar Dommenget^{1*}, Kerry Nice^{1,4}, Tobias Bayr², Dieter Kasang³, Christian
7 Stassen¹ and Mike Rezny¹

8
9 *: corresponding author; dietmar.dommenget@monash.edu

10 1: Monash University, School of Earth, Atmosphere and Environment, Clayton, Victoria
11 3800, Australia.

12 2: GEMOAR Helmholtz Centre for Ocean Research, Düsternbrooker Weg 20, 24105 Kiel,
13 Germany

14 3: DKRZ, Hamburg, Germany

15 4: Transport, Health, and Urban Design Hub, Faculty of Architecture, Building, and
16 Planning, University of Melbourne, Victoria 3010, Australia

17
18 submitted the Geoscientific Model Development, 8 March 2018
19

20 **Abstract**

21 This study introduces the Monash Simple Climate Model (MSCM) experiment
22 database. The model simulations are based on the Globally Resolved Energy
23 Balance (GREB) model. They provide a basis to study three different aspects of
24 climate model simulations: (1) understanding the processes that control the
25 mean climate, (2) the response of the climate to a doubling of the CO₂
26 concentration, and (3) scenarios of external CO₂ concentration and solar
27 radiation forcings. A series of sensitivity experiments in which elements of the
28 climate system are turned off in various combinations are used to address (1)
29 and (2). This database currently provides more than 1,300 experiments and has
30 an online web interface for fast analysis of the experiments and for open access
31 to the data. We briefly outline the design of all experiments, give a discussion of
32 some results, and put the findings into the context of previously published
33 results from similar experiments. We briefly discuss the quality and limitations
34 of the MSCM experiments and also give an outlook on possible further
35 developments. The GREB model simulation of the mean climate processes is
36 quite realistic, but does have uncertainties in the order of 20-30%. The GREB
37 model without flux corrections has a root mean square error in mean state of
38 about 10°C, which is larger than those of general circulation models (2°C).
39 However, the MSCM experiments show good agreement to previously published
40 studies. Although GREB is a very simple model, it delivers good first-order



41 estimates, is very fast, highly accessible, and can be used to quickly try many
42 different sensitivity experiments or scenarios.
43

44 1. Introduction

45 Our understanding of the dynamics of the climate system and climate changes is
46 strongly linked to the analysis of model simulations of the climate system using a
47 range of climate models that vary in complexity and sophistication. Climate
48 model simulations help us to predict future climate changes and they help us
49 gain a better understand of the dynamics of this complex system.

50 State-of-the-art climate models, such as used in the Coupled Model Inter-
51 comparison Project (CMIP; Taylor et al. 2012), are highly complex simulations
52 that require significant amounts of computing resources and time. Such model
53 simulations require a significant amount of preparation. The development of
54 idealized experiments that would help in the understanding and modelling of
55 climate system processes are often difficult to realize with the complex CMIP-
56 type climate models. In this context, simplified climate models are useful, as they
57 provide a fast first guess that help to inform more complex models. They also
58 help in understanding the interactions in the complex system.

59 In this article, we introduce the Monash Simple Climate Model (MSCM) database
60 (version: MSCM-DB v1.0). The MSCM is an interactive website
61 (<http://mscm.dkrz.de>, Germany and [http://monash.edu/research/simple-
62 climate-model](http://monash.edu/research/simple-climate-model), Australia) and database that provide access to a series of more
63 than 1,300 experiments with the Globally Resolved Energy Balance (GREB)
64 model [Dommenget and Floter 2011; here after referred to as DF11]. The GREB
65 model was primarily developed to conceptually understand the physical
66 processes that control the global warming pattern in response to an increase in
67 CO_2 concentration. It therefore centres around the surface temperature (T_{surf})
68 tendency equation and simulates only the processes needed for resolving the
69 global warming pattern.

70 Simplified climate models, such as Earth System Models of Intermediate
71 Complexity (EMICs), often aim at reducing the complexity to increase the
72 computation speed and therefore allow faster model simulations (e.g. CLIMBER
73 [Petoukhov et al. 2000], UVic [Weaver et al. 2001], FAMOUS [A] or LOVECLIM
74 [Goosse et al. 2010]). These EMICs are very similar in structure to state-of-the-
75 art Coupled General Circulation Models (CGCMs), following the approach of
76 simulating the geophysical fluid dynamics. The GREB model differs, in that it
77 follows an energy balance approach and does not simulate the geophysical fluid
78 dynamics of the atmosphere. It is therefore a climate model that does not include
79 weather dynamics, but focusses on the long term mean climate and its response
80 to external boundary changes.

81 The purpose of the MSCM database for research studies are the following:

- 82
- 83 • **First Guess:** The MSCM provides first guesses for how the climate may
84 change in idealized or realistic experiments. The MSCM experiments can
85 be used to test ideas before implementing and testing them in more
86 detailed CGCM simulations.



- 87 • **Null Hypothesis:** The simplicity of the GREB model provides a good null
88 hypothesis for understanding the climate system. Because it does not
89 simulate weather dynamics or circulation changes of neither large nor
90 small scale it provides the null hypothesis of a climate as a pure energy
91 balance problem.
- 92 • **Conceptual understanding:** The simplicity of the GREB model helps to
93 better understand the interactions in the complex climate and, therefore,
94 helps to formulate simple conceptual models for climate interactions.
- 95 • **Education:** Studying the results of the MSCM helps to understand the
96 interactions that control the mean state climate and its regional and
97 seasonal differences. It helps to understand how the climate will respond
98 to external forcings in a first-order approximation.
- 99

100 The MSCM provides interfaces for fast analysis of the experiments and selection
101 of the data (see Figs. 1-3). It is designed for teaching and outreach purposes, but
102 also provides a useful tool for researchers. The focus in this study will be on
103 describing the research aspects of the MSCM, whereas the teaching aspects of it
104 will not be discussed. The MSCM experiments focus on three different aspects of
105 climate model simulations: (1) understanding the processes that control the
106 mean climate, (2) the response of the climate to a doubling of the CO_2
107 concentration, and (3) scenarios of external CO_2 concentration and solar
108 radiation forcings. We will provide a short outline of the design of all
109 experiments, give a brief discussion of some results, and put the findings into
110 context of previously published literature results from similar experiments.

111 The DF11 study focussed primarily on the development of the model equations
112 and the discussion of the response pattern to an increase in CO_2 concentration.
113 This study here will give a more detailed discussion on the performance of the
114 GREB model on simulation of the mean state climate.

115 The paper is organized as follows: The following section describes the GREB
116 model, the experiment designs, the MSCM interface, and the input data used. A
117 short analysis of the experiments is given in section 3. This section will mostly
118 focus on the GREB model performance in comparison to observations and
119 previously published simulations in the literature, but it will also give some
120 indications of the findings in the model experiments and the limitations of the
121 GREB model. The final section will give a short summary and outlook for
122 potential future developments and analysis.

123 2. Model and experiment descriptions

124 The GREB model is the underlying modelling tool for the MSCM interface. The
125 development of the model and all equations have been presented in DF11. The
126 model is simulating the global climate on a horizontal grid of 3.75° longitude x
127 3.75° latitude and in three vertical layers: surface, atmosphere and subsurface
128 ocean. It simulates the main physical processes that control the surface
129 temperature tendencies: solar (short-wave) and thermal (long-wave) radiation,
130 the hydrological cycle (including evaporation, moisture transport and
131 precipitation), horizontal transport of heat and heat uptake in the subsurface
132 ocean. Atmospheric circulation and cloud cover are seasonally prescribed
133 boundary condition, and state-independent flux corrections are used to keep the



134 GREB model close to the observed mean climate. Thus, the GREB model does not
135 simulate the atmospheric or ocean circulation and is therefore conceptually very
136 different from CGCM simulations.

137 The model does simulate important climate feedbacks such as the water vapour
138 and ice-albedo feedback, but an important limitation of the GREB model is that
139 the response to external forcings or model parameter perturbations do not
140 involve circulation or cloud feedbacks, which are relevant in CGCM simulations
141 [Bony et al. 2006].

142 Input climatologies (e.g. T_{surf} or atmospheric humidity) for the GREB model are
143 taken from the NCEP reanalysis data from 1950-2008 [Kalnay et al. 1996], cloud
144 cover climatology from the ISCCP project [Rossow and Schiffer 1991], ocean
145 mixed layer depth climatology from Lorbacher et al. [2006], and topographic
146 data was taken from ECHAM5 atmosphere model [Roeckner et al. 2003].

147 GREB does not have any internal (natural) variability since daily weather
148 systems are not simulated. Subsequently, the control climate or response to
149 external forcings can be estimated from one single year. The primary advantage
150 of the GREB model in the context of this study is its simplicity, speed, and low
151 computational cost. A one year GREB model simulation can be done on a
152 standard PC computer in about 1 s (about 100,000 simulated years per day). It
153 can do simulations of the global climate much faster than any state-of-the-art
154 climate model and is therefore a good first guess approach to test ideas before
155 they are applied to more complex CGCMs. A further advantage is the lag of
156 internal variability which allows the detection of a response to external forcing
157 much more easily.

158 a. Experiments for the mean climate deconstruction

159 The conceptual deconstruction of the GREB model to understand the interactions
160 in the climate system that lead to the mean climate characteristics is done by
161 defining 11 processes (switches; see Fig. 1). For each of these switches, a term in
162 the model equations is set to zero or altered if the switch is "OFF". The processes
163 and how they affect the model equations are briefly listed below (with a short
164 summary in Table 1). The model equations relevant for the experiments in this
165 study are briefly restated in the appendix section A1 for the purpose of
166 explaining each experimental setup in the MSCM.

167

168

169 **Ice-albedo:** The surface albedo (α_{surf}) and the heat capacity over ocean points
170 (γ_{surf}) are influenced by snow and sea ice cover. In the GREB model these are a
171 direct function of T_{surf} . When the Ice-albedo switch is OFF the surface albedo of
172 all points is constant (0.1) and, for ocean points, γ_{surf} follows the prescribed
173 ocean mixed layer depth independent of T_{surf} (i.e. no ice-covered ocean).

174

175 **Clouds:** The cloud cover, CLD , influences the amount of solar radiation absorbed
176 at the surface (α_{clouds} in eq. [A5]) and the emissivity of the atmospheric
177 layer, ϵ_{atmos} , for thermal radiation (eq. [A8]). When the Clouds switch is OFF, the
178 cloud cover is set to zero.

179

180 **Oceans:** The ocean in the GREB simulates subsurface heat storage with the
181 surface mixed layer (~upper 50-100m). When the ocean switch is OFF, the F_{ocean}



182 term in eq. [A1] is set to zero, eq. [A3] is set to zero and the heat capacity of all
183 ocean points is set to that of land points.

184

185 **Atmosphere:** The atmosphere in the GREB model simulates a number of
186 processes: The hydrological cycle, horizontal transport of heat, thermal
187 radiation, and sensible heat exchange with the surface. When the atmosphere
188 switch is OFF, eq. [A2] and [A4] are set to zero, the heat flux terms, F_{sense} and
189 F_{latent} in eq. [A1] are set to zero and the downward atmospheric thermal
190 radiation term in eq. [A6] is set to zero.

191

192 **Diffusion of Heat:** The atmosphere transports heat by isotropic diffusion (4th
193 term in eq. [A2]). When this process is switched OFF, the term is set to zero.

194

195 **Advection of Heat:** The atmosphere transports heat by advection following the
196 mean wind field, \vec{u} (5th term in eq. [A2]). When this process is switched OFF, the
197 term is set to zero.

198

199 **CO₂:** The CO₂ concentration affects the emissivity of the atmosphere, ε_{atmos} (eq.
200 [A9]). When this process is switched OFF, the CO₂ concentration is set to zero.

201

202 **Hydrological cycle:** The hydrological cycle in the GREB model simulates the
203 evaporation, precipitation, and transport of atmospheric water vapour. It further
204 simulates latent heat cooling at the surface and heating in the atmosphere. When
205 the hydrological cycle is switched OFF, eq. [A4] is set to zero, the heat flux term
206 F_{latent} in eq. [A1] is set to zero, and $viwv_{atmos}$ in eq. [A9] is set to zero.
207 Subsequently, atmospheric humidity is zero.

208 It needs to be noted here, that the atmospheric emissivity in the log-function
209 parameterization of eq. [A9] can become negative, if the hydrological cycle, cloud
210 cover and CO₂ concentration are switched OFF (set to zero). This marks an
211 unphysical range of the GREB emissivity function and we will discuss the
212 limitations of the GREB model in these experiments in Section 3b.

213

214 **Diffusion of Water Vapour:** The atmosphere transports water vapour by
215 isotropic diffusion (3rd term in eq. [A4]). When this process is switched OFF, the
216 term is set to zero.

217

218 **Advection of Water Vapour:** The atmosphere transports heat by advection
219 following the mean wind field, \vec{u} (5th term in eq. [A2]). When this process is
220 switched OFF, the term is set to zero.

221

222 **Model Corrections:** The model correction terms in eqs. [A1, A3 and A4]
223 artificially force the mean T_{surf} , T_{atmos} , and q_{air} climate to be as observed. When
224 the model correction is switched OFF, the three terms are set to zero. This will
225 allow the GREB model to be studied without any artificial corrections and
226 therefore help to evaluate the GREB model equations' skill in simulating the
227 climate dynamics.

228 It should be noted here that the model correction terms in the GREB model have
229 been introduced to study the response to doubling of the CO₂ concentration for
230 the current climate, which is a relative small perturbation if compared against



231 the other perturbations considered above. They are meaningful for a small
232 perturbation in the climate system, but are less likely to be meaningful when
233 large perturbations to the climate system are done (e.g. cloud cover set to zero).

234
235 Each different combination of the above-mentioned process switches defines a
236 different experiment. However, not all combinations of switches are possible,
237 because some of the process switches are depending on each other (see Table 1
238 and Fig. 1). The total number of experiments possible with these process
239 switches is 656. For each experiment, the GREB model is run for 50 years,
240 starting from the original GREB model climatology and the final year is
241 presented as the climatology of this experiment in the MSCM database.

242 **b. Experiments for the 2xCO₂ response deconstruction**

243 The conceptual deconstruction of the GREB model to understand the interactions
244 in the climate system that lead to the climate response to a doubling of the CO₂
245 concentration can be done in a similar way, as described above for the mean
246 climate. However, there are a number of differences that need to be considered.
247 A meaningful deconstruction of the response to a doubling of the CO₂
248 concentration should consider the reference control mean climate since the
249 forcings and the feedbacks controlling the response are mean state dependent.
250 We therefore ensure that all sensitivity experiments in this discussion have the
251 same reference mean control climate. This is achieved by estimating the flux
252 correction term in eqs. [A1, A3 and A4] for each sensitivity experiment to
253 maintain the observed control climate. Thus, when a process is switched OFF, the
254 control climatological tendencies in eqs. [A1, S3 and S4] are the same as in the
255 original GREB model, but changes in the tendencies due to external forcings, such
256 as doubling of the CO₂ concentration are not affected by the disabled process.
257 This is the same approach as in DF11.

258 For the 2xCO₂ response deconstruction experiments, we define 10 boundary
259 conditions or processes (switches; see Fig. 2). The Ice-albedo, advection and
260 diffusion of heat and water vapour, and the hydrological cycle processes are
261 defined in the same way as for the mean climate deconstruction (section 2a). The
262 remaining boundary conditions and processes are briefly listed below (and a
263 short summary is given in Table 2).

264
265 The following boundary conditions are considered:

266
267 **Topography:** The topography in the GREB model affects the amount of
268 atmosphere above the surface and therefore affects the emissivity of the
269 atmosphere in the thermal radiation (eq. [A9]). Regions with high topography
270 have less CO₂ concentration in the thermal radiation (eq. [A9]). When the
271 topography is turned OFF, all points of the GREB model are set to sea level height
272 and have the same amount of CO₂ concentration in the thermal radiation (eq.
273 [A9]).

274
275 **Clouds:** The cloud cover in the GREB model affects the incoming solar radiation
276 and the emissivity of the atmosphere in the thermal radiation (eq. [A9]). In
277 particular, it influences the sensitivity of the emissivity to changes in the CO₂
278 concentration. A clear sky atmosphere is more sensitive to changes in the CO₂



279 concentration than a fully cloud-covered atmosphere. When the cloud cover
280 switch is OFF, the observed cloud cover climatology boundary conditions are
281 replaced with a constant global mean cloud cover of 0.7. It is not set to zero to
282 avoid an impact on the global climate sensitivity, and to focus on the regional
283 effects of inhomogeneous cloud cover.

284
285 **Humidity:** Similarly, to the cloud cover, the amount of atmospheric water
286 vapour affects the emissivity of the atmosphere in the thermal radiation and, in
287 particular, the sensitivity to changes in the CO_2 concentration (eq. [A9]). A humid
288 atmosphere is less sensitive to changes in the CO_2 concentration than a dry
289 atmosphere. When the humidity switch is OFF, the constraint to the observed
290 humidity climatology (flux correction in eq. [A4]) is replaced with a constant
291 global mean humidity of 0.0052 [kg/kg]. It is again not set to zero to avoid an
292 impact on the global climate sensitivity, but to focus on the regional effects of
293 inhomogeneous humidity.

294
295 The additional feedbacks and processes considered are:

296
297 **Ocean heat uptake:** The ocean heat uptake in GREB is done in two ocean layers.
298 The largest part of the ocean heat is in the subsurface layer, T_{ocean} (eq. [A3]).
299 When the ocean switch is OFF the F_{ocean} term in eq. [A1] is set to zero, equation
300 [A3] is set to zero and the heat capacity (γ_{surf}) off all ocean points in eq. [A1] is
301 set to that of a 50m water column.

302
303 The total number of experiments with these process switches is 640. For each
304 experiment, the GREB model is run for 50 years, starting from the original GREB
305 model climatology and the changes relative to the original GREB model
306 climatology of this experiment is presented in the MSCM database.

307 c. Scenario experiments

308 A number of different scenarios of external boundary condition changes exist in
309 the MSCM experiment database. They include different changes in the CO_2
310 concentration and in the incoming solar radiation. A complete overview is given
311 in Table 3. A short description follows below.

312 RCP-scenarios

313 In the Representative Concentration Pathways (RCP) scenarios the GREB model
314 is forced with time varying CO_2 concentrations. All five different simulations have
315 the same historical time evolution of CO_2 concentrations starting from 1850 to
316 2000, and from 2001 follow the RCP8.5, RCP6, RCP4.5, RCP2.6 and the A1B CO_2
317 concentration pathways until 2100 [van Vuuren et al. 2011].

318 Idealized CO_2 scenarios

319
320 The 15 idealized CO_2 concentration scenarios in the MSCM experiment database
321 focus on the non-linear time delay and regional differences in the climate
322 response to different CO_2 concentrations. These were implemented in five
323 simulations in which the control CO_2 concentration (340ppm) was changed in
324 the first time step to a scaled CO_2 concentration of 0, 0.5, 2, 4, and 10 times the
325



326 control level. The $0.5\times CO_2$ and $2\times CO_2$ simulations are 50yrs long and the others
327 are 100yrs long.

328 Two different simulations with idealized time evolutions of CO_2 concentrations
329 are conducted to study the time delay of the climate response. In one simulation,
330 the CO_2 concentration is doubled in the first time step, held at this level for 30yrs
331 then returned to control levels instantaneously. In the second simulation, the CO_2
332 concentration is varied between the control and $2\times CO_2$ concentrations following
333 a sine function with a period of 30yrs, starting at the minimum of the sine
334 function at the control CO_2 concentration. Both simulations are 100yrs long.

335 The third set of idealized CO_2 concentration scenarios double the CO_2
336 concentrations restricted to different regions or seasons. The eight regions and
337 seasons include: the Northern or Southern Hemisphere, tropics ($30^\circ S$ - $30^\circ N$) or
338 extra-tropics (poleward of 30°), land or oceans and in the month October to
339 March or in the month April to September. Each experiment is 50yrs long.

340

341 **Solar radiation**

342 Two different experiments with changes in the solar constant were created. In
343 the first experiment, the solar constant is increased by about 2% ($+27W/m^2$),
344 which leads to about the same global warming as a doubling of the CO_2
345 concentration [Hansen et al. 1997]. In the second experiment, the solar constant
346 oscillates at an amplitude of $1W/m^2$ and a period of 11yrs, representing an
347 idealized variation of the incoming solar short wave radiation due to the natural
348 11yr solar cycle [Willson and Hudson 1991]. Both experiments are 50yrs long.

349

350 **Idealized orbital parameters**

351 A series of five simulations are done in the context of orbital forcings and the
352 related ice age cycles. In one simulation, the incoming solar radiation as function
353 of latitude and day of the year was changed to its values as it was 231Kyr ago
354 [Berger and Loutre 1991 and Huybers 2006]. In an additional simulation, the CO_2
355 concentration is reduced from 340ppm to 200ppm as observed during the peak
356 of ice age phases in combination with the incoming solar radiation changes. Both
357 simulations are 100yrs long.

358 In three sensitivity experiments, we changed the incoming solar radiation
359 according to some idealized orbital parameter changes to study the effect of the
360 most important orbital parameters. The orbital parameters changed are: the
361 distance to the sun, the Earth axis tilt relative to the Earth-Sun plane (obliquity)
362 and the eccentricity of the Earth orbit around the sun. The orbit radius was
363 changed from 0.8AU to 1.2AU in steps of 0.01AU, the obliquity from -25° to 90° in
364 steps of 2.5° and the eccentricity from 0.3 (Earth closest to the sun in July) to 0.3
365 (Earth furthest from the sun in July) in steps of 0.01. Each sensitivity experiment
366 was started from the control GREB model (1AU radius, 23.5° obliquity and 0.017
367 eccentricity) and run for 50yrs. The last year of each simulation is presented as
368 the estimate for the equilibrium climate.

369 **3. Some results of the model simulations**

370 The MSCM experiment database includes a large set of experiments that address
371 many different aspects of the climate. At the same time, the GREB model has
372 limited complexity and not all aspects of the climate system are simulated in the



373 GREB experiments. The following analysis will give a short overview of some of
374 the results that can be taken from the MSCM experiments. In this we will focus
375 on aspects of general interest and on comparing the outcome to results of other
376 published studies to illustrate the strength and limitations of the GREB model in
377 this context. The discussion, however, will be incomplete, as there are simply too
378 many aspects that could be discussed in this set of experiments. We will
379 therefore focus on a general introduction and leave space for future studies to
380 address other aspects.

381 **a. GREB model performance**

382 The skill of the GREB model is illustrated in Figure 4, by running the GREB model
383 without the correction terms. For reference, we compare this GREB run with the
384 observed mean climate and seasonal cycle (this is identical to running the GREB
385 model with correction terms) and with a bare world. The latter is the GREB
386 model with all switches OFF (radiative balance without an atmosphere and a
387 dark surface). In comparison with the full GREB model, this illustrates how much
388 all the climate processes affect the climate.

389 The GREB model without correction terms does capture the main features of the
390 zonal mean climate, the seasonal cycle, the land-sea contrast and even smaller
391 scale structures within continents or ocean basins (e.g. seasonal cycle structure
392 within Asia or zonal temperature gradients within ocean basins). For most of the
393 globe (<50° from the equator), the GREB model root-mean-squared error (RMSE)
394 for the annual mean T_{surf} is less than 10°C relative to the observed (see Fig. 4g).
395 This is larger than for state-of-the-art CMIP-type climate models, which typically
396 have an RMSE of about 2°C [Dommenget 2012]. In particular, the regions near
397 the poles have high RMSE. It seems likely that the meridional heat transport is
398 the main limitation in the GREB model, given the too warm tropical regions and
399 the, in general, too cold polar regions and the too strong seasonal cycle in the
400 polar regions in the GREB model without correction terms.

401 The GREB model performance can be put in perspective by illustrating how
402 much the climate processes simulated in the GREB model contribute to the mean
403 climate relative to the bare world simulation (see Fig. 4). The GREB RMSE to
404 observed is about 20-30% of the RMSE of the bare world simulation (not
405 shown), suggesting that the GREB model has a relative error of about 20-30% in
406 the processes that it simulates or due to processes that it does not simulate (e.g.
407 ocean heat transport).

408 **b. Mean climate deconstruction**

409 Understanding what is causing the mean observed climate with its regional and
410 seasonal difference is often central for understanding climate variability and
411 change. For instance, the seasonal cycle is often considered as a first guess
412 estimate for climate sensitivity [Knutti et al. 2006]. In the following analysis, we
413 will give a short overview on how the 10 processes of the MSCM experiments
414 contribute to the mean climate and its seasonal cycle.

415 In Figures 5 and 6 the contribution of each of the 10 processes (except the
416 atmosphere) to the annual mean climate (Fig. 5) and its seasonal cycle (Fig. 6)
417 are shown. In each experiment, all processes are active, but the process of
418 interest and the model correction terms are turned OFF. The results are
419 compared against the complete GREB model without the model correction terms



420 (all processes active; expect model correction terms). For the hydrological we
421 will discuss some additional experiments in which the ice-albedo feedback is
422 turned OFF as well.

423 The Ice/Snow cover (Fig. 5a) has a strong cooling effect mostly at the high
424 latitudes in the cold season, which is due to the ice-albedo feedback. However, in
425 the warm season (not shown) the insulation effect of the sea ice actually leads to
426 warming, as the ocean cannot cool down as much during winter as it does
427 without sea ice.

428 Clouds (Fig. 5b) have a large net cooling effect globally due to the solar radiation
429 reflection effect dominating over the thermal radiation warming effect. It is also
430 interesting to note that the strongest cooling effect of cloud cover is over regions
431 with fairly little cloud cover (e.g. deserts and mountain regions). This is due to
432 the interaction with other climate feedbacks such as the water vapour feedback.
433 Previous studies on the cloud cover effect on the overall climate mostly focus on
434 the radiative forcings estimates, but to our best knowledge do not present the
435 overall change in surface temperature [e.g. Rossow and Zhang 1995].

436 The large ocean heat capacity slows down the seasonal cycle (Fig. 6c).
437 Subsequently, the seasons are more moderate than they would be without the
438 ocean transferring heat from warm to cold seasons. This is, in particular,
439 important in the mid and higher latitudes. The effect of the ocean heat capacity,
440 however, has also an annual mean warming effect (Fig. 5c). This is due to the
441 non-linear thermal radiation cooling. The non-linear black body negative
442 radiation feedback is stronger for warmer temperatures, which are not reached
443 in a moderated seasonal cycle with the larger ocean heat capacity.

444 The diffusion of heat reduces temperature extremes (Fig. 5d). It therefore warms
445 extremely cold regions (e.g. polar regions) and cools the hottest regions (e.g.
446 warm deserts). In global averages, this is mostly cancelled out. The advection of
447 heat has strong effects where the mean winds blow across strong temperature
448 gradients. This is mostly present in the Northern Hemisphere (Fig. 5e). The most
449 prominent feature is the strong warming of the northern European and Asian
450 continents in the cold season. In global average, warming and cooling mostly
451 cancel out.

452 The CO_2 concentration leads to global averages, warming of about 9 degrees (Fig.
453 5f). Even though it is the same CO_2 concentration everywhere, the warming effect
454 is different at different locations. This is discussed in more detail in DF11 and in
455 section 3c.

456 The input of water vapour into the atmosphere by the hydrological cycle leads to
457 a substantial amount of warming globally (Fig. 5g). However, we need to
458 consider that the experiment with switching OFF the hydrological cycle is the
459 only experiment in which we have a significant amount of global cooling (by
460 about $-44^\circ C$). As a result, most of the earth is below freezing temperatures and
461 therefore has a much stronger ice-albedo feedback than in any other experiment.
462 This leads to a significant amplification of the response.

463 It is instructive to repeat the experiments with the ice-albedo feedback switched
464 OFF (see supplementary Fig. 1). In these experiments, all processes show a
465 reduced impact on the annual mean temperatures, but the hydrological cycle is
466 most strongly affected by it. The ice-albedo effect almost doubles the
467 hydrological cycle response, while for all other processes the effect is about a
468 10% to 40% increase. In the following discussions, we will therefore consider



469 the hydrological cycle impact with and without ice-albedo feedback. In the
470 average of both response (Fig. 5g and SFig. 1g) the hydrological cycle has a global
471 mean impact of about +34°C with strongest amplitudes in the tropics. It is still
472 the strongest of all processes.

473 Similar to the oceans, it dampens the seasonal cycle (Fig. 6g), but with a much
474 weaker amplitude. The transport of water vapour away from warm and moist
475 regions (e.g. tropical oceans) to cold and dry regions (e.g. high latitudes and
476 continents) leads to additional warming in the regions that gain water vapour
477 and cooling to those that lose water vapour (Fig. 6h). The effect is similar in both
478 hemispheres. The transport of water vapour along the mean wind directions has
479 stronger effects on the Northern Hemisphere than on the Southern Hemisphere,
480 since the northern hemispheric mean winds have more of a meridional
481 component, which creates advection across water vapour gradients (Fig. 6i). This
482 effect is most pronounced in the cold seasons.

483 Most processes have a predominately zonal structure. We can therefore take a
484 closer look at the zonal mean climate and seasonal cycle of all processes to get a
485 good representation of the relative importance of each process, see Fig. 7. The
486 annual mean climate is most strongly influenced by the hydrological cycle (here
487 shown as the mean of the response with and without the ice-albedo feedback).
488 The cloud cover has an opposing cooling effect, but is weaker than the warming
489 effect of the hydrological cycle. The warming effect by the ocean's heat capacity
490 is similar in scale to that of the CO_2 concentration.

491 The seasonal cycle is damped most strongly by the ocean's heat capacity and by
492 the hydrological cycle. The later may seem unexpected, but is due to the effect
493 that the increased water vapour has a stronger warming effect in the cold
494 seasons, similarly to the greenhouse effect of CO_2 concentrations. In turn, the
495 ice/snow cover and cloud cover lead to an intensification of the seasonal cycle at
496 higher latitudes. Again, the later may seem unexpected, but is due to the
497 interaction with other climate feedbacks such as the water vapour feedback,
498 which also makes the climate more strongly respond to changes in cloud cover in
499 regions where there actually is very little cloud cover (e.g. deserts).

500 As an alternative way of understanding the role of the different process we can
501 build up the complete climate by introducing one process after the other, see
502 Figs. 8 and 9. We start with the bare earth (e.g. like our Moon) and then
503 introduce one process after the other. The order in which the processes are
504 introduced is mostly motivated by giving a good representation for each of the
505 10 processes. However, it can also be interpreted as a build up the Earth climate
506 in a somewhat historical way: We assume that initially the earth was a bare
507 planet and then the atmosphere, ocean, and all the other aspects were build up
508 over time.

509 The Bare Earth (all switches OFF) is a planet without atmosphere, ocean or ice. It
510 has an extremely strong seasonal cycle (Fig. 9a) and is much colder than our
511 current climate (Fig. 8a). It also has no regional structure other than meridional
512 temperature gradients. The combination of all climate processes will create most
513 of the regional and seasonal difference that make our current climate.

514 The atmospheric layer in the GREB model simulates two processes, if all other
515 processes are turned off: a turbulent sensible heat exchange with the surface and
516 thermal radiation due to residual trace gasses other than CO_2 , water vapour or
517 clouds. However, as mentioned in the appendix A1 the log-function



518 approximation leads to negative emissivity if all greenhouse gasses (CO_2 and
519 water vapour) concentrations and cloud cover are zero. The negative emissivity
520 turns the atmospheric layer into a cooling effect, which dominates the impact of
521 the atmosphere in this experiment (Figs. 8b, c). This is a limitation of the GREB
522 model and the result of this experiment as such should be considered with
523 caution. In a more realistic experiment we can set the emissivity of the
524 atmosphere to zero or a very small value (0.01) to simulate the effect of the
525 atmosphere without CO_2 , water vapour and cloud cover, see SFig. 2. Both
526 experiments have very similar warming effects in polar regions. Suggesting that
527 the sensible heat exchange warms the surface. The residual thermal radiation
528 effect from the emissivity of 0.01 has only a minor impact (SFig. 2f and g).
529 The warming effect of the CO_2 concentration is nearly uniform (Figs. 8d, e) and
530 without much of a seasonal cycle (Figs. 9d, e), if all other processes are turned
531 OFF. This accounts for a warming of about $+9^\circ\text{C}$.
532 The oceans slow down the seasonal cycle by their large heat capacity (Figs. 9f, g).
533 The effective heat capacity of the oceans is proportional to the observed mixed
534 layer in the GREB model, which causes some small variations (differences from
535 the zonal means) as seen in the seasonal cycle of the oceans. Land points are not
536 affected, since no atmospheric transport exist (advection and diffusion turned
537 OFF). The different heat capacity between oceans and land already make a
538 significant element of the regional and seasonal climate differences (Figs. 8f, g).
539 Introducing turbulent diffusion of heat in the atmosphere now enables
540 interaction between points, which has the strongest effects along coastlines and
541 in higher latitudes (Figs. 8h, i). It reduces the land-sea contrast and has strong
542 effects over land with warming in winter and cooling in summer (Figs. 9h, i). The
543 extreme climates of the winter polar region are most strongly affected by the
544 turbulent heat exchange with lower latitudes. The turbulent heat exchange
545 makes the regional climate difference again a bit more realistic.
546 The advection of heat is strongly dependent on the temperature gradients along
547 the mean wind field directions. It provides substantial heating during the winter
548 season for Europe, Russia, and western North America (Figs. 8j, k, 9j, k). The
549 structure (differences from the zonal mean) created by this process is mostly
550 caused by the prescribed mean wind climatology. In particular, the milder
551 climate in Europe compared to northeast Asia on the same latitudes, are created
552 by wind blowing from the ocean onto land. The same is true for the differences
553 between the west and east coasts of the northern North America. The climate
554 regional and seasonal structures are now already quite realistic, but the overall
555 climate is much too cold. The ice/snow cover further cools the climate, in
556 particular, the polar regions (Figs. 8l, m). This difference illustrates that the ice-
557 albedo feedback is primarily leading to cooling in higher latitudes and mostly in
558 the winter season.
559 Introducing the hydrological cycle brings the most important greenhouse gas
560 into the atmosphere: water vapour. This has an enormous warming effect
561 globally (Figs. 8n, o) and a moderate reduction in the strength of the seasonal
562 cycle (Figs. 9n, o). The resulting modelled climate is now much too warm, but
563 introducing the cloud cover cools the climate substantially (Figs. 8p, q) and leads
564 to a fairly realistic climate.
565 The atmospheric transport (diffusion and advection) brings water vapour from
566 relative moist regions to relatively dry regions (Figs. 8r, s). This leads to



567 enhanced warming in the dry and cold regions (e.g. Sahara Desert or polar
568 regions) by the water vapour thermal radiation (greenhouse) effect and cooling
569 in the regions where it came from (e.g. tropical oceans). The heating effect is
570 similar to the transport of heat and has also a strong seasonal cycle component.

571 **c. $2\times CO_2$ response deconstruction**

572 The doubling of the CO_2 concentrations leads to a distinct warming pattern with
573 polar amplification, a land-sea contrast and significant seasonal differences in
574 the warming rate. These structures in the warming pattern reflect the complex
575 interactions between feedbacks in the climate system and regional difference in
576 CO_2 forcing pattern. The MSCM $2\times CO_2$ response experiments are designed to help
577 understand the interactions causing this distinct warming pattern. DF11
578 discussed many aspects of these experiments with focus on the land-sea
579 contrast, the seasonal differences, and the polar amplification. We therefore will
580 focus here only on some aspects that have not been previously discussed in
581 DF11.

582 In the GREB model, we can turn OFF the atmospheric transport and therefore
583 study the local interaction without any lateral interactions. Figure 10 shows
584 three experiments in which the atmospheric transport and other processes (see
585 Figure caption) are inactive. The three experiments highlight the regional
586 difference in the CO_2 forcing pattern and in the two main feedbacks (water
587 vapour and ice-albedo).

588 In the first experiment (Fig. 10a) without feedback processes, the local T_{surf}
589 response is approximately directly proportional to the local CO_2 forcing. The
590 regional differences are caused by differences in the cloud cover and
591 atmospheric humidity, since both influence the thermal radiation effect of CO_2
592 [DF11, Kiehl and Ramanathan 1982 and Cess et al. 1993]. This causes, on
593 average, the land regions to see a stronger forcing than oceanic regions (see Fig.
594 10b). However, even over oceans we can see clear differences. For instance, the
595 warm pool of the western tropical Pacific sees less CO_2 forcing than the eastern
596 tropical Pacific.

597 The ice-albedo feedback is strongly localized and it is strongest over the mid-
598 latitudes of the northern continents and at the sea ice edge of around Antarctica
599 (Figs. 10c and d). The water vapour feedback is far more wide-spread and
600 stronger (Figs. 10e and f). It is strongest in relatively warm and dry regions (e.g.
601 subtropical oceans), but also shows some clear localized features, such as the
602 strong Arabian or Mediterranean Seas warming.

603 **d. Scenarios**

604 The set of scenario experiments in the MSCM simulations allows us to study the
605 response of the climate system to changes in the external boundary conditions in
606 a number of different ways. In the following, we will briefly illustrate some
607 results from these scenarios and organize the discussion by the different themes
608 in scenario experiments.

609 The CMIP project has defined a number of standard CO_2 concentration projection
610 simulations, that give different RCP scenarios for the future climate change, see
611 Fig. 11a. The GREB model sensitivity in these scenarios is similar to those of the
612 CMIP database [Forster et al. 2013].



613 Idealized CO_2 concentration scenarios help to understand the response to the CO_2
614 forcing. In Figure 11b, we show the global mean T_{surf} response to different scaling
615 factors of CO_2 concentrations. To first order, we can see that the global mean T_{surf}
616 response follows a logarithmic CO_2 concentration (e.g. any doubling of the CO_2
617 concentration leads to the same global mean T_{surf} response; compare $2xCO_2$ with
618 $4xCO_2$ or with in Fig.11b) as suggested in other studies [Myhre et al. 1998].
619 However, this relationship does breakdown if we go to very low CO_2
620 concentrations (e.g. zero CO_2 concentration) illustrating that the log-function
621 approximation of the CO_2 forcing effect is only valid within a narrow range far
622 away from zero CO_2 concentration.

623 The transient response time to CO_2 forcing can be estimated from idealized CO_2
624 concentration changes, see Fig. 11c. The step-wise change in CO_2 concentration
625 illustrates the response time of the global climate. In the GREB model, it takes
626 about 10yrs to get 80% of the response to a CO_2 concentration change (see step-
627 function response, Fig. 11c). In turn, the response to a CO_2 concentration wave
628 time evolution is a lag of about 3yrs. The fast versus slow response also leads to
629 different warming patterns with strong land-sea contrasts (not shown), that are
630 largely similar to those found in previous studies [Held et al. 2010].

631 The regional aspects of the response to a CO_2 concentration can also be studied
632 by partially increasing the CO_2 concentration in different regions, see Fig. 12. The
633 warming response mostly follows the regions where we partially changed the
634 CO_2 concentration, but there are some interesting variations in this. The partial
635 increase in the CO_2 concentration over oceans has a stronger warming impact
636 than the partial increase in the CO_2 concentration over land for most Southern
637 Hemisphere land regions. In turn, the land forcing has little impact for the ocean
638 regions. The boreal winter forcing has stronger impact on the Southern
639 Hemisphere than boreal summer forcing, suggesting that the warm season
640 forcing is, in general, more important than the cold season forcing. The only
641 exception to this is the Tibet-plateau region.

642 A series of scenarios focus on the impact of solar forcing. In Figure 11d, we show
643 the response to an idealized 11yr solar cycle. The global mean T_{surf} response is
644 two orders of magnitude smaller than the response to a doubling of the CO_2
645 concentration, reflecting the weak amplitude of this forcing. This result is largely
646 consistent with the response found in GCM simulations [Cubasch et al. 1997], but
647 does not consider possible more complicated amplification mechanisms [Meehl
648 et al. 2009]. A change in the solar constant of $+27W/m^2$ has a global T_{surf}
649 warming response similar to a doubling of the CO_2 concentration, but with a
650 slightly different warming pattern, see Fig. 13. The warming pattern of a solar
651 constant change has a stronger warming where incoming sun light is stronger
652 (e.g. tropics or summer season) and a weaker warming in region with less
653 incoming sun light (e.g. higher latitudes or winter season). This is in general
654 agreement with other modelling studies [Hansen et al. 1997].

655 On longer paleo time scales ($>10,000$ yrs), changes in the orbital parameters
656 affect the incoming sun light. Figure 14 illustrates the response to a number of
657 orbital solar radiation changes. Incoming radiation (sunlight) typical of the ice
658 age (231kyrs ago) has less incoming sunlight in the Northern Hemispheric
659 summer. However, it has every little annual global mean changes (Fig. 14a) due
660 to increases in sunlight over other regions and seasons. The T_{surf} response
661 pattern in the zonal mean at the different seasons is very similar to the solar



662 forcing, but the response is slightly more zonal and seasonal differences are less
663 dominant (Fig. 14b). The response is also amplified at higher latitudes. However,
664 in the global mean there is no significant global cooling as observed during ice
665 ages. If the solar forcing is combined with a reduction in the CO_2 concentration
666 (from 340ppm to 200ppm), we find a global mean cooling of $-1.7^\circ C$ (Fig. 14c),
667 which is still much weaker than observed during ice ages, but is largely
668 consistent with previous studies of simulations of ice age conditions [Weaver et
669 al. 1998, Braconnot et al. 2007]. This is not unexpected since the GREB model
670 does not include an ice sheet model and, therefore, does not include glacier
671 growth feedbacks that would amplify ice age cycles.

672 A better understanding of the orbital solar radiation forcing can be gained by
673 analysing the response to idealized orbital parameter changes. We therefore
674 vary the Earth distance to the sun (radius), the earth axis tilt to the earth orbit
675 plane (obliquity) and shape of the earth orbit around the sun (eccentricity) over
676 a wider range, see Figs. 14 d-f. When the radius is changed by 10%, the Earth
677 climate becomes essentially uninhabitable, with either global mean temperature
678 above $30^\circ C$ (approx. summer mean temperature of the Sahara) or a completely
679 ice-covered snowball Earth. This suggests that the habitable zone of the Earth
680 radius is fairly small due to the positive feedbacks within the climate system
681 simulated in the GREB model (not considering long-term or more complex
682 atmospheric chemistry feedbacks) and largely consistent with previous studies
683 [Kasting et al. 1993].

684 When the obliquity is zero, the tropics become warmer and the polar regions
685 cool down further than today's climate, as they now receive very little sunlight
686 throughout the whole year. In the extreme case, when the obliquity is 90° , the
687 tropics become ice covered and cooler than the polar regions, which are now
688 warmer than the tropics today and ice free. The polar regions now have an
689 extreme seasonal cycle (not shown), with sunlight all day during summer and no
690 sunlight during winter. Any eccentricity increase in amplitude would lead to a
691 warmer overall climate. Thus, a perfect circle orbit around the sun has, on
692 average, the coldest climate and all of the more extreme eccentricity (elliptic)
693 orbits have warmer climates. This suggests that the warming effect of the section
694 of the orbit that has a closer transit around the sun in an eccentricity orbit
695 relative to the perfect circle orbit overcompensates the cooling effect of the more
696 remote transit around the sun in the other half of the orbit relative to the perfect
697 circle orbit.

698 **4. Summary and discussion**

699 In this study, we introduced the MSCM database (version: MSCM-DB v1.0) for
700 research analysis with more than 1,300 experiments. It is based on model
701 simulations with the GREB model for studies of the processes that contribute to
702 the mean climate, the response to doubling of the CO_2 concentration, and
703 different scenarios with CO_2 or solar radiation forcings. The GREB model is a
704 simple climate model that does not simulate internal weather variability,
705 circulation, or cloud cover changes. It provides a simple and fast null hypothesis
706 for the interactions in the climate system and its response to external forcings.

707 The GREB model without flux corrections simulates the mean observed climate
708 well and has an uncertainty of about $10^\circ C$. The model has larger cold biases in



709 the polar regions indicating that the meridional heat transport is not strong
710 enough. Relative to a bare world without any climate processes the RMSE is
711 reduced to about 20-30% relative to observed. Thus, as a first guess, it can be
712 assumed that the GREB model simulations gives a 20-30% uncertainty in the
713 processes it simulates. Further, the GREB models emissivity function reaches
714 unphysical negative values when water vapour, CO₂ and cloud cover is set to
715 zero. This is a limitation of the log-function parametrization, that can potentially
716 be revised if a new parameterization is developed that considers these cases.
717 However, it is beyond the scope of this study to develop such a new
718 parameterization and it is left for future studies.

719 The MSCM experiments for the conceptual deconstruction of the observed mean
720 climate provide a good understanding of the processes that control the annual
721 mean climate and its seasonal cycle. The cloud cover, atmospheric water vapour,
722 and the ocean heat capacity are the most important processes that determine the
723 regional difference in the annual mean climate and its seasonal cycle. The
724 observed seasonal cycle is strongly damped not only by the ocean heat capacity,
725 but also by the water vapour feedback. In turn, ice-albedo and cloud cover
726 amplify the seasonal cycle in higher latitudes.

727 The conceptual deconstruction of the response to a doubling of the CO₂
728 concentration based on the MSCM experiments has mostly been discussed in
729 DF11, but some additional results shown here focused on the local forcing in
730 response without horizontal interaction. It has been shown here that the CO₂
731 forcing has a clear land-sea contrast, supporting the land-sea contrast in the T_{surf}
732 response. The water vapour feedback is wide-spread and most dominant over
733 the subtropical oceans, whereas the ice-albedo feedback is more localized over
734 Northern Hemispheric continents and around the sea ice border.

735 The series of scenario simulations with CO₂ and solar forcing provide many
736 useful experiments to understand different aspects of the climate response. The
737 RCP and idealized CO₂ forcing scenarios give good insights into the climate
738 sensitivity, regional differences, transient effects, and the role of CO₂ forcing at
739 different seasons or locations. The solar forcing experiments illustrate the subtle
740 differences in the warming pattern to a CO₂ forcing and the orbital solar forcing
741 illustrated elements of the climate response to long term, paleo, climate forcings.

742 In summary, the MSCM provides a wide range of experiments for understanding
743 the climate system and its response to external forcings. It builds a basis on
744 which conceptual ideas can be tested to a first-order and it provides a null
745 hypothesis for understanding complex climate interactions. Some of the
746 experiments presented here are similar to previously published simulations. In
747 general, the GREB model results agree well with the results of more complex
748 GCM simulations. It is beyond the scope of this study to discuss all aspects of the
749 experiments and their results. This will be left to future studies.

750 Future development of this MSCM database will continue and it is expected that
751 this database will grow. The development will go in several directions: the GREB
752 model performance in the processes that it currently simulates will be further
753 improved. In particular, the simulation of the hydrological cycle needs to be
754 improved to allow the use of the GREB model to study changes in precipitation.
755 Simulations of aspects of the large-scale atmospheric circulation, aerosols,
756 carbon cycle, or glaciers would further enhance the GREB model and would
757 provide a wider range of experiments to run for the MSCM database.



758 **5. Code availability**

759 The MSCM model code, including all required input files, to do all experiments
760 described on the MSCM homepage and in this paper, can be downloaded as
761 compressed tar archive from the MSCM homepage under

762
763 <http://mscm.dkrz.de/download/mscm-web-code.tar.gz>

764
765 or from the bitbucket repository under

766
767 <https://bitbucket.org/tobiasbayr/mscm-web-code>

768
769 The data for all the experiments of the MSCM can be accessed via the MSCM
770 webpage interface (DOI: 10.4225/03/5a8cadac8db60). The mean
771 deconstruction experiments file names have an 11 digits binary code that
772 describe the 11 process switches combination: 1=ON and 0=OFF. The digit from
773 left to right present the following processes:

- 774
- 775 1. Model corrections
 - 776 2. Ice albedo
 - 777 3. Cloud cover
 - 778 4. Advection of water vapour
 - 779 5. Diffusion of water vapour
 - 780 6. Hydrologic cycle
 - 781 7. Ocean
 - 782 8. CO₂
 - 783 9. Advection of heat
 - 784 10. Diffusion of heat
 - 785 11. Atmosphere

786
787 For example, the data file *greb.mean.decon.exp-1011111111.gad* is the
788 experiment with all processes ON, but ice albedo is OFF. The 2x CO₂ response
789 deconstruction experiments file names have a 10 digits binary code that describe
790 the 10 process switches combination. The digit from left to right present the
791 following processes:

- 792
- 793 1. Ocean heat uptake
 - 794 2. Advection of water vapour
 - 795 3. Diffusion of water vapour
 - 796 4. Hydrologic cycle
 - 797 5. ice albedo
 - 798 6. Advection of heat
 - 799 7. Diffusion of heat
 - 800 8. Humidity (climatology)
 - 801 9. Clouds (climatology)
 - 802 10. Topography (Observed)

803
804 For example, the data file *response.exp-0111111111.2xCO2.gad* is the experiment
805 with all processes ON, but ocean heat uptake is OFF. The individual experiments
806 can be chosen from the webpage interface by selecting the desired switch



807 combinations. Alternatively, all experiments can be downloaded in a combined
808 tar-file from the webpage interface.
809

810 **Acknowledgments**

811 This study was supported by the ARC Centre of Excellence for Climate System
812 Science, Australian Research Council (grant CE110001028).

813 **References**

- 814 Berger, A., and M. F. Loutre, 1991: Insolation Values for the Climate of the Last
815 1000000 Years. *Quaternary Sci Rev*, **10**, 297-317.
- 816 Bony, S., and Coauthors, 2006: How well do we understand and evaluate climate
817 change feedback processes? *Journal of Climate*, **19**, 3445-3482.
- 818 Braconnot, P., and Coauthors, 2007: Results of PMIP2 coupled simulations of the
819 Mid-Holocene and Last Glacial Maximum - Part 1: experiments and large-
820 scale features. *Clim Past*, **3**, 261-277.
- 821 Cess, R. D., and Coauthors, 1993: Uncertainties in Carbon-Dioxide Radiative
822 Forcing in Atmospheric General-Circulation Models. *Science*, **262**, 1252-
823 1255.
- 824 Cubasch, U., R. Voss, G. C. Hegerl, J. Waszkewitz, and T. J. Crowley, 1997:
825 Simulation of the influence of solar radiation variations on the global
826 climate with an ocean-atmosphere general circulation model. *Climate
827 Dynamics*, **13**, 757-767.
- 828 Dommenges, D., 2012: Analysis of the Model Climate Sensitivity Spread Forced
829 by Mean Sea Surface Temperature Biases. *Journal of Climate*, **25**, 7147-
830 7162.
- 831 Dommenges, D., and J. Floter, 2011: Conceptual understanding of climate change
832 with a globally resolved energy balance model. *Climate Dynamics*, **37**,
833 2143-2165.
- 834 Forster, P. M., T. Andrews, P. Good, J. M. Gregory, L. S. Jackson, and M. Zelinka,
835 2013: Evaluating adjusted forcing and model spread for historical and
836 future scenarios in the CMIP5 generation of climate models. *Journal of
837 Geophysical Research-Atmospheres*, **118**, 1139-1150.
- 838 Goosse, H., and Coauthors, 2010: Description of the Earth system model of
839 intermediate complexity LOVECLIM version 1.2. *Geosci Model Dev*, **3**, 603-
840 633.
- 841 Hansen, J., M. Sato, and R. Ruedy, 1997: Radiative forcing and climate response.
842 *Journal of Geophysical Research-Atmospheres*, **102**, 6831-6864.
- 843 Held, I. M., M. Winton, K. Takahashi, T. Delworth, F. R. Zeng, and G. K. Vallis, 2010:
844 Probing the Fast and Slow Components of Global Warming by Returning
845 Abruptly to Preindustrial Forcing. *Journal of Climate*, **23**, 2418-2427.
- 846 Huybers, P., 2006: Early Pleistocene glacial cycles and the integrated summer
847 insolation forcing. *Science*, **313**, 508-511.
- 848 Kalnay, E., and Coauthors, 1996: The NCEP/NCAR 40-year reanalysis project.
849 *Bulletin of the American Meteorological Society*, **77**, 437-471.
- 850 Kasting, J. F., D. P. Whitmire, and R. T. Reynolds, 1993: Habitable Zones around
851 Main-Sequence Stars. *Icarus*, **101**, 108-128.
- 852 Kiehl, J. T., and V. Ramanathan, 1982: Radiative Heating Due to Increased Co₂ -
853 the Role of H₂O Continuum Absorption in the 12-18 Mu-M Region. *Journal
854 of the Atmospheric Sciences*, **39**, 2923-2926.
- 855 Knutti, R., G. A. Meehl, M. R. Allen, and D. A. Stainforth, 2006: Constraining
856 climate sensitivity from the seasonal cycle in surface temperature. *Journal
857 of Climate*, **19**, 4224-4233.
- 858 Lorbacher, K., D. Dommenges, P. P. Niiler, and A. Kohl, 2006: Ocean mixed layer
859 depth: A subsurface proxy of ocean-atmosphere variability. *Journal of
860 Geophysical Research-Oceans*, **111**, -.



- 861 Meehl, G. A., J. M. Arblaster, K. Matthes, F. Sassi, and H. van Loon, 2009:
862 Amplifying the Pacific Climate System Response to a Small 11-Year Solar
863 Cycle Forcing. *Science*, **325**, 1114-1118.
- 864 Myhre, G., E. J. Highwood, K. P. Shine, and F. Stordal, 1998: New estimates of
865 radiative forcing due to well mixed greenhouse gases. *Geophysical*
866 *Research Letters*, **25**, 2715-2718.
- 867 Petoukhov, V., A. Ganopolski, V. Brovkin, M. Claussen, A. Eliseev, C. Kubatzki, and
868 S. Rahmstorf, 2000: CLIMBER-2: a climate system model of intermediate
869 complexity. Part I: model description and performance for present
870 climate. *Climate Dynamics*, **16**, 1-17.
- 871 Roeckner, E., and Coauthors, 2003: The atmospheric general circulation model
872 ECHAM 5. Part I: Model description. *Reports of the Max-Planck-Institute*
873 *for Meteorology*, **349**.
- 874 Rossow, W. B., and R. A. Schiffer, 1991: Isccp Cloud Data Products. *Bulletin of the*
875 *American Meteorological Society*, **72**, 2-20.
- 876 Rossow, W. B., and Y. C. Zhang, 1995: Calculation of Surface and Top of
877 Atmosphere Radiative Fluxes from Physical Quantities Based on Isccp
878 Data Sets .2. Validation and First Results. *Journal of Geophysical Research-*
879 *Atmospheres*, **100**, 1167-1197.
- 880 Taylor, K. E., R. J. Stouffer, and G. A. Meehl, 2012: An Overview of Cmp5 and the
881 Experiment Design. *Bulletin of the American Meteorological Society*, **93**,
882 485-498.
- 883 van Vuuren, D. P., and Coauthors, 2011: The representative concentration
884 pathways: an overview. *Climatic Change*, **109**, 5-31.
- 885 Weaver, A. J., M. Eby, F. F. Augustus, and E. C. Wiebe, 1998: Simulated influence of
886 carbon dioxide, orbital forcing and ice sheets on the climate of the Last
887 Glacial Maximum. *Nature*, **394**, 847-853.
- 888 Weaver, A. J., and Coauthors, 2001: The UVic Earth System Climate Model: Model
889 description, climatology, and applications to past, present and future
890 climates. *Atmosphere-Ocean*, **39**, 361-428.
- 891 Willson, R. C., and H. S. Hudson, 1991: The Suns Luminosity over a Complete
892 Solar-Cycle. *Nature*, **351**, 42-44.

893

894



$$940 \quad Fa_{thermal} = \sigma T_{surf}^4 - 2\varepsilon_{atmos}\sigma T_{atmos-rad}^4 \quad [A7]$$

941

942 The emissivity of the atmosphere, ε_{atmos} , is a function of the cloud cover, CLD ,943 the atmospheric water vapour, $viwv_{atmos}$, and the CO_2 , CO_2^{topo} , concentration

944

$$945 \quad \varepsilon_{atmos} = \frac{pe_8 - CLD}{pe_9} \cdot (\varepsilon_0 - pe_{10}) + pe_{10} \quad [A8]$$

946

947 with

948

$$949 \quad \varepsilon_0 = pe_4 \cdot [pe_1 \cdot CO_2^{topo} + pe_2 \cdot viwv_{atmos} + pe_3] \\ 950 \quad \quad \quad + pe_5 \cdot [pe_1 \cdot CO_2^{topo} + pe_3] + pe_6 \cdot [pe_2 \cdot viwv_{atmos} + pe_3] + pe_7 \quad [A9]$$

951

952 The first three terms in the eq. [A9] represent different spectral bands in which

953 the thermal radiation of water vapour and the CO_2 are active. In the first term954 both are active, in the second only CO_2 and in the third only water vapour. The

955 combined effect of eqs. [A8] and [A9] is that the sensitivity of the emissivity to

956 CO_2 is depending on the presents of cloud cover and water vapour.

957 It is important to note that this log-function parametrization of the emissivity is

958 an approximation developed in DF11 for $2xCO_2$ -concentration experiments.

959 While the parametrization may be a good approximation for a wide range of the

960 greenhouse gasses, it is likely to have limited skill in extreme variation of the

961 greenhouse gasses. For instance, if all greenhouse gasses (CO_2 and water vapour)

962 concentrations and cloud cover are zero then the emissivity of the atmospheric

963 layer in eq. [A9] becomes -0.26. This is not a physically meaningful value and

964 experiments in which all greenhouse gasses (CO_2 and water vapour) and cloud

965 cover are zero need to be analysed with caution. The analysis section will discuss

966 these limitations in these experiments.

967 **Tables**

968

969 **Table 1:** Processes (switches) controlled in the sensitivity experiment for the
 970 mean climate deconstruction. Indentation in the left column indicates processes
 971 switches are dependent on the switches above being ON.

Mean Climate Deconstruction	
Name	Description
Ice-albedo	controls surface albedo (α_{surf}) and heat capacity (γ_{surf}) at sea ice points as function of T_{surf}
Clouds	controls cloud cover climatology. OFF equals no clouds.
Oceans	controls F_{ocean} term in eq. [A1] and the heat capacity (γ_{surf}) off all ocean points. OFF equals no F_{ocean} and as γ_{surf} over land.
Atmosphere	controls sensible heat flux (F_{sense}) and the downward atmospheric thermal radiation term in eq. [A6].
Diffusion of Heat	controls diffusion of heat
Advection of Heat	controls advection of heat
CO ₂	controls CO ₂ concentration
Hydrological cycle	controls atmospheric humidity. OFF equals zero humidity
Diffusion of water vapour	controls diffusion of water vapour
Advection of water vapour	controls advection of water vapour
Model Corrections	controls model flux correction terms

972

973

974



975

976 **Table 2:** Processes (switches) controlled in the sensitivity experiment for the977 2xCO₂ response deconstruction. Indentation in the left column indicates

978 processes switches are dependent on the switches above being ON.

979

2xCO ₂ Response Deconstruction	
Boundary Conditions	
Name	Description
Topography (Observed)	controls topography effect on thermal radiation. OFF equals all land point on sea level.
Clouds (climatology)	controls cloud cover climatology. OFF equals 0.7 cloud cover everywhere.
Humidity (climatology)	controls the humidity constraint. OFF equals a control humidity 0.0052 [kg/kg] everywhere. Humidity can still respond to forcings.
Feedbacks/Processes	
Diffusion of Heat	controls diffusion of heat
Advection of Heat	controls advection of heat
Ice-albedo	controls surface albedo (α_{surf}) and heat capacity (γ_{surf}) at sea ice points as function of T_{surf}
Ocean heat uptake	controls F_{ocean} term in eq. [A1] and the heat capacity (γ_{surf}) off all ocean points. OFF equals no F_{ocean} and γ_{surf} of a 50m water column.
Hydrological cycle	controls atmospheric humidity. OFF equals zero humidity
Diffusion of water vapour	controls diffusion of water vapour
Advection of water vapour	controls advection of water vapour

980

981

982

983



984 **Table 3:** List of scenario experiments.

RCP CO ₂ -scenarios		
Name	length	Description
Historical	1850-2000	CO ₂ -concentration following the historical scenario
RCP8.5	2001-2100	CO ₂ -concentration following the RCP8.5 scenario
RCP6	2001-2100	CO ₂ -concentration following the RCP6 scenario
RCP4	2001-2100	CO ₂ -concentration following the RCP4 scenario
RCP3PD	2001-2100	CO ₂ -concentration following the RCP3PD scenario
A1B	2001-2100	CO ₂ -concentration following the A1B scenario
Idealized CO ₂ concentrations		
Zero-CO ₂	100yrs	zero CO ₂ concentrations
0.5xCO ₂	50yrs	140ppm CO ₂ concentrations
2xCO ₂	50yrs	560ppm CO ₂ concentrations
4xCO ₂	100yrs	1120ppm CO ₂ concentrations
10xCO ₂	100yrs	2800ppm CO ₂ concentrations
Partial CO ₂ concentrations		
CO ₂ -N-hemis	50yrs	2xCO ₂ only in the northern hemisphere
CO ₂ -S-hemis	50yrs	2xCO ₂ only in the southern hemisphere
CO ₂ -tropics	50yrs	2xCO ₂ only between 30°S and 30°N
CO ₂ -extra-tropics	50yrs	2xCO ₂ only poleward of 30°
CO ₂ -oceans	50yrs	2xCO ₂ only over ice-free ocean points
CO ₂ -land	50yrs	2xCO ₂ only over land and sea ice points
CO ₂ -winter	50yrs	2xCO ₂ only in the month Oct. to Mar.
CO ₂ -summer	50yrs	2xCO ₂ only in the month Apr. to Sep.
Solar radiation		
solar+27W/m ²	50yrs	solar constant increased by +27W/m ²
11yrs-solar	50yrs	solar idealized solar constant 11yrs cycle
Orbital parameter		
Solar-231Kyr	100yrs	incoming solar radiation according to orbital parameters 231Kyr ago.
Solar-231Kyr-200ppm	100yrs	as Solar-231Kyr, but with CO ₂ concentrations decreased from 280ppm to 200ppm.
Orbit-radius	40steps	equilibrium response to different Earth orbit radius from 0.8AU to 1.2AU.
Obliquity	45steps	equilibrium response to different Earth axis tilt from -25° to 90°
Eccentricity	60steps	equilibrium response to different Earth orbit eccentricity from 0.3 to 0.3

985

986

987



988 **Table A1:** Variables of the GREB model equations.

Variable	Dimensions	Description
T_{surf}	x, y, t	surface temperature
T_{atmos}	x, y, t	atmospheric temperature
T_{ocean}	x, y, t	subsurface ocean temperature
q_{air}	x, y, t	atmospheric humidity
γ_{surf}	x, y, t	heat capacity of the surface layer
γ_{atmos}	x, y, t	heat capacity of the atmosphere
γ_{ocean}	x, y, t	heat capacity of the subsurface ocean
F_{solar}	x, y, t	solar radiation absorbed at the surface
$F_{thermal}$	x, y, t	thermal radiation into the surface
$F_{a_{thermal}}$	x, y, t	thermal radiation into the atmospheric
F_{latent}	x, y, t	latent heat flux into the surface
Q_{latent}	x, y, t	latent heat flux into the atmospheric
F_{sense}	x, y, t	sensible heat flux from the atmosphere into the surface
$F_{O_{sense}}$	x, y, t	sensible heat flux from the subsurface ocean into the surface layer
F_{ocean}	x, y, t	sensible heat flux from the subsurface ocean
$F_{correct}$	x, y, t	heat flux corrections for the surface
$F_{O_{correct}}$	x, y, t	heat flux corrections for the subsurface ocean
$q_{correct}$	x, y, t	mass flux corrections for the atmospheric humidity
$\Delta T_{o_{entrain}}$	x, y, t	subsurface ocean temperature tendencies by entrainment
Δq_{eva}	x, y, t	mass flux for the atmospheric humidity by evaporation
Δq_{precip}	x, y, t	mass flux for the atmospheric humidity by precipitation
α_{surf}	x, y, t	albedo of the surface layer
ϵ_{atmos}	x, y, t	emissivity of the atmosphere
$T_{atmos-rad}$	x, y, t	atmospheric radiation temperature
$viwv_{atmos}$	x, y, t	atmospheric column water vapour mass
κ	constant	isotropic diffusion coefficient
pe_i	constant	empirical emissivity function parameters
\vec{u}	x, y, t _j	horizontal wind field
α_{clouds}	x, y, t _j	albedo of the atmosphere
h_{mld}	x, y, t _j	Ocean mixed layer depth
r	y, t _j	fraction of incoming sunlight (24hrs average)
CO_2^{topo}	x, y	CO ₂ concentration scaled by topographic elevation
S_0	constant	solar constant
σ	constant	Stefan-Boltzman constant
t _j	-	day within the annual calendar
Δt	constant	model integration time step
σ	constant	Stefan-Boltzmann constant

989

990 **Figures**

991

992

993

994

995

996

997

998

999

1000

1001

1002

1003

1004

1005

1006

1007

1008

1009

1010

1011

1012

1013

1014

1015

1016

1017

1018

1019

1020

1021

1022

1023

1024

1025

1026

1027

1028

1029

1030

1031

1032

1033

1034

1035

1036

1037

1038

Figure 1. MSCM interface running the deconstruction of the mean climate experiments. The experiment A, on the left, has all processes turned ON and experiment B, on right, has all turned OFF. The T_{surf} of Experiment A is shown in the upper left map, Exp. B in the upper right and the difference between both in the lower map. The example shows the values for the October mean.

Figure 2. MSCM interface running the deconstruction of the response to a doubling of the CO_2 concentration experiments. The experiment A, on the left, has all processes turned ON and experiment B, on right, has all turned OFF. The T_{surf} response of Experiment A is shown in the upper left map, Exp. B in the upper right and the difference between both in the lower map. The example shows the annual mean values after 28yrs.

Figure 3. Examples of the MSCM scenario interface. (a) presenting a single scenario (here RCP 8.5 CO_2 forcing) and (b) the comparison of two different scenarios (here a CO_2 forcing is compared against a change in the solar constant by $+27W/m^2$).

Figure 4. T_{surf} annual mean (upper row) and seasonal cycle (half the difference between mean of July to September minus January to March; middle row) for three different experiments: GREB with all processes turned OFF (Bare Earth), all processes on (observed) and only the correction term OFF (GREB). The zonal mean of the annual mean (g) and seasonal cycle (h) of the three experiments in comparison with the zonal mean RMSE of the GREB model without correction terms relative to observed.

Figure 5. Changes in the annual mean T_{surf} in the GREB model simulations with different processes turned OFF as described in section 2a relative to the complete GREB model without model correction terms: (a) Ice/Snow, (b) clouds, (c) oceans, (d) heat advection, (e) heat diffusion, (f) CO_2 concentration, (g) hydrological cycle, (h) diffusion of water vapour and (i) advection of water vapour. Global mean differences are shown in the headings. Differences are for the control minus the sensitivity experiment (positive indicates the control experiment is warmer). All values are in $^{\circ}C$. In some panels, the values are scaled for better comparison: (b), (c) and (f) by a factor of 2, (a), (d) and (e) by a factor of 3, and (h) and (i) by a factor of 6.

Figure 6. As in Fig. 5, but for the seasonal cycle. The mean seasonal cycle is defined by the difference between the month [JAS] - [JFM] divided by two. Positive values on the North hemisphere indicate stronger seasonal cycle in the sensitivity experiments than in the full GREB model. Vice versa for the Southern Hemisphere. Global root mean square differences are shown in the headings. All values are in $^{\circ}C$. In some panels, the values are scaled for better comparison: (b), (d) and (e) by a factor of 2, and (h) and (i) by a



1039 factor of 10. (g) is the mean for the hydrological cycle experiments with
1040 and without the ice-albedo process active.

1041
1042 **Figure 7.** Zonal mean values of the annual mean (a) and seasonal cycle
1043 differences (b) for the experiments as shown in Figs. 5 and 6. g) The mean
1044 for the hydrological cycle is for the experiments with and without the ice-
1045 albedo process active.

1046
1047 **Figure 8.** Conceptual build-up of the annual mean climate: starting with all
1048 processes turned OFF (a) and then adding more processes in each row:
1049 (b) atmosphere, (d) CO₂, (f) oceans, (h) heat diffusion, (j) heat advection,
1050 (l) hydrological cycle, (n) ice-albedo, (p) clouds and (r) water vapour
1051 transport. The panels on the right column show the difference of the left
1052 panel to the previous row left panel. Global mean values are shown in the
1053 heading. All values are in °C. In some panels in the right column the values
1054 are scaled for better comparison: (e), (g) and (q) by a factor of 2, (i) by
1055 a factor of 3 and (k), (o) and (s) by a factor of 4. For details see on the
1056 experiments see section 2a.

1057
1058 **Figure 9.** As in Fig. 8, but conceptual build-up of the seasonal cycle. The
1059 seasonal cycle is defined by the difference between the month [JAS] -
1060 [JFM] divided by two. Global mean absolute values are shown in the
1061 heading. In some panels in the right column the values are scaled for
1062 better comparison: (c), (i), (m) and (o) by a factor of 2, (k), (q) and (s) by
1063 a factor of 5 and for (e) by a factor of 30.

1064
1065 **Figure 10.** Local T_{surf} response to doubling of the CO₂ concentration in
1066 experiments without atmospheric transport (each point on the maps is
1067 independent of the others). (a) GREB with topography, humidity and
1068 cloud processes and all other processes OFF. (b) Difference of (a) to GREB
1069 with topography and all other processes OFF scaled by a factor of 10. (c)
1070 GREB model as in (a), but with ice-albedo process ON. (d) Difference of
1071 (c)-(a) scaled by a factor of 2. (e) GREB model as in (a), but with
1072 hydrological cycle process ON. (f) Difference of (e)-(a) scaled by a factor
1073 of 2. For details see on the experiments see section 2b.

1074
1075 **Figure 11.** Global mean T_{surf} response to idealized forcing scenarios:
1076 (a) different RCP CO₂ forcing scenarios. (b) Scaled CO₂ concentrations. (c)
1077 idealized CO₂ concentration time evolutions (dotted lines) and the
1078 respective T_{surf} responses (solid lines of the same colour). (d) idealized
1079 11yrs solar cycle. List of experiments is given in Table 3.

1080
1081 **Figure 12.** T_{surf} response to partial doubling of the CO₂ concentration
1082 in: Northern (a) and Southern (b) hemisphere, tropics (d) and extra-
1083 tropics (e), oceans (g) and land (h), and in boreal winter (j) and summer
1084 (k). The right column panels show the difference between the two panels
1085 two the left in the same row.

1086



1087 **Figure 13.** T_{surf} response to changes in the solar constant by $+27\text{W/m}^2$
1088 (middle column) versus a doubling of the CO_2 concentration (left column)
1089 for the annual mean (upper) and the seasonal cycle (lower). The seasonal
1090 cycle is defined by the difference between the month [JAS] - [JFM] divided
1091 by two. The right column panels show the difference between the two
1092 panels two the left in the same row scaled by 4 (c) and 3 (f).

1093 **Figure 14.** Orbital parameter forcings and T_{surf} responses: (a) incoming
1094 solar radiation changes in the Solar-231Kyr experiment relative to the
1095 control GREB model. T_{surf} response in Solar-231Kyr (b) and Solar-231Kyr-
1096 200ppm (c) relative to the control GREB model. Annual mean T_{surf} in
1097 Orbit-radius (d), Obliquity (e) and Eccentricity (f). The solid vertical line
1098 in (d)-(f) marks the control (today) GREB model.



Figure 1

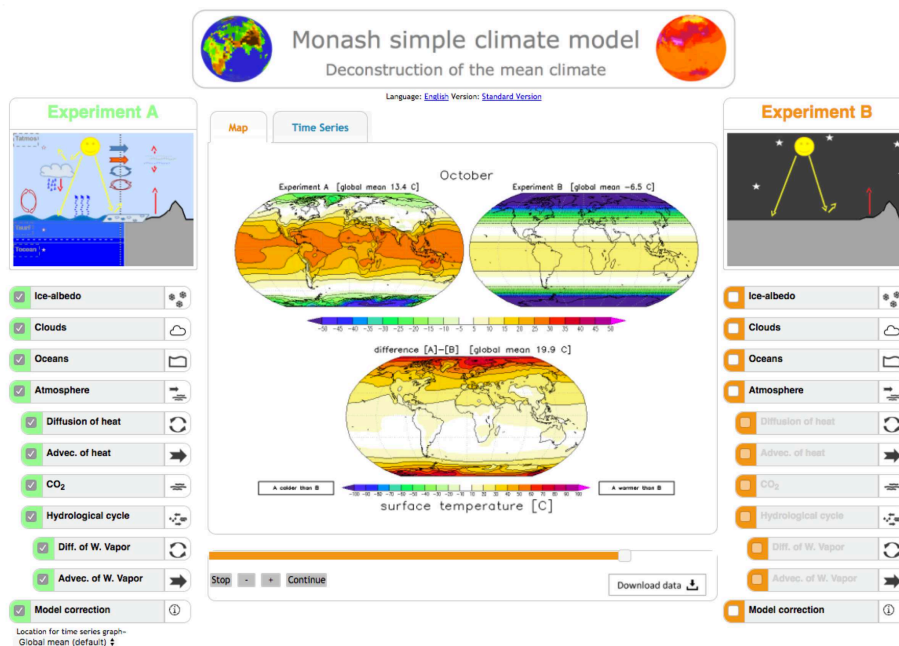


Figure 1: MSCM interface running the deconstruction of the mean climate experiments. The experiment A, on the left, has all processes turned ON and experiment B, on right, has all turned OFF. The T_{surf} of Experiment A is shown in the upper left map, Exp. B in the upper right and the difference between both in the lower map. The example shows the values for the October mean.



Figure 2

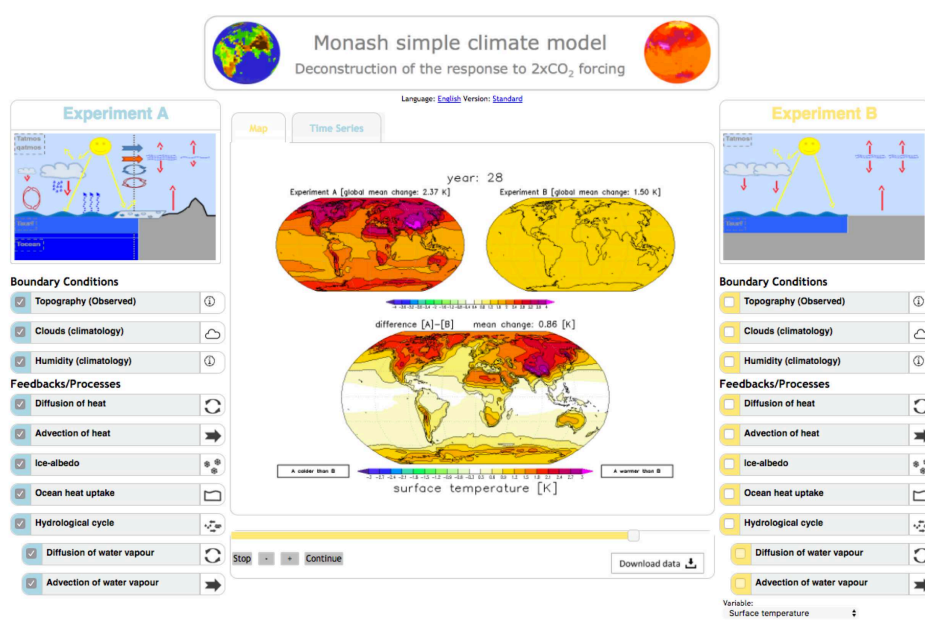
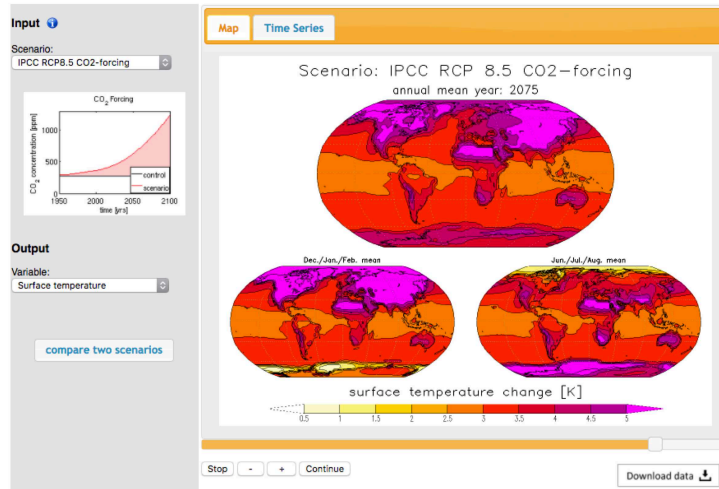


Figure 2: MSCM interface running the deconstruction of the response to a doubling of the CO_2 concentration experiments. The experiment A, on the left, has all processes turned ON and experiment B, on right, has all turned OFF. The T_{surf} response of Experiment A is shown in the upper left map, Exp. B in the upper right and the difference between both in the lower map. The example shows the annual mean values after 28yrs.



Figure 3

(a)



(b)

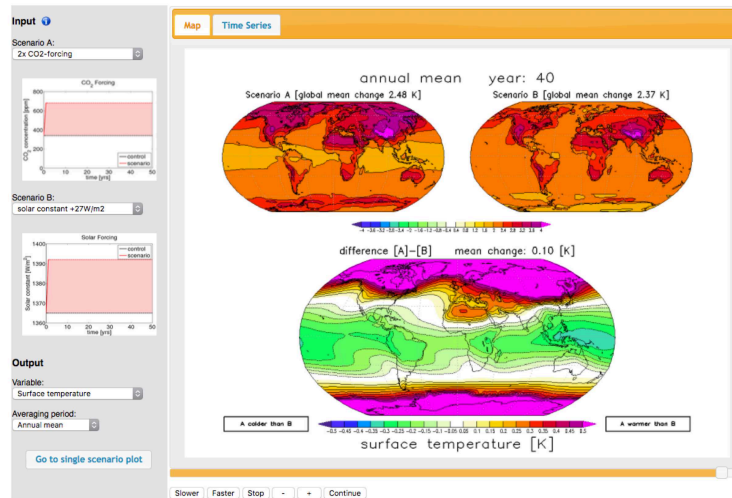


Figure 3: Examples of the MSCM scenario interface. (a) presenting a single scenario (here RCP 8.5 CO_2 forcing) and (b) the comparison of two different scenarios (here a CO_2 forcing is compared against a change in the solar constant by $+27W/m^2$).



Figure 4

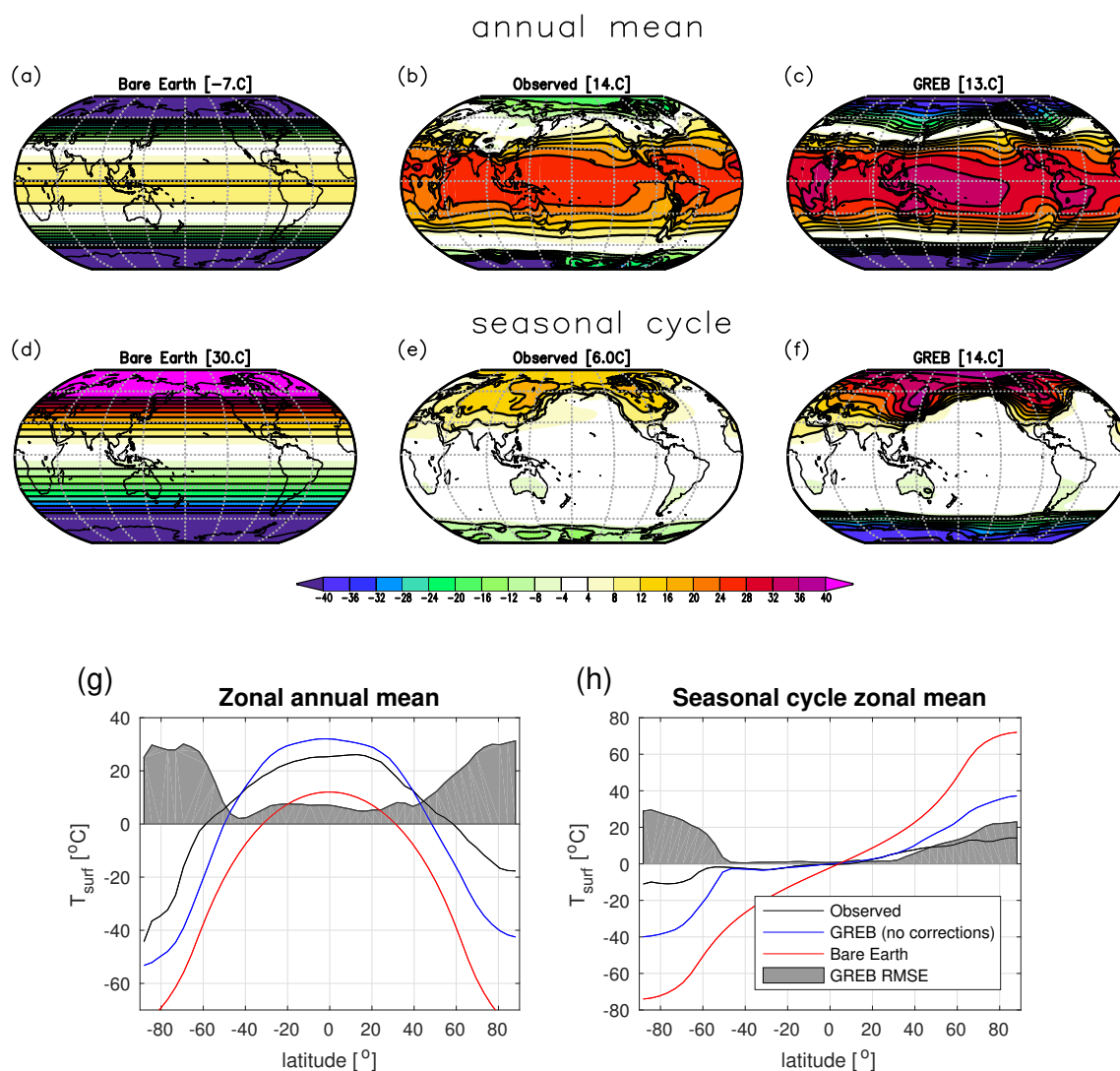


Figure 4: T_{surf} annual mean (upper row) and seasonal cycle (half the difference between mean of July to September minus January to March; middle row) for three different experiments: GREB with all processes turned OFF (Bare Earth), all processes on (observed) and only the correction term OFF (GREB). The zonal mean of the annual mean (g) and seasonal cycle (h) of the three experiments in comparison with the zonal mean RMSE of the GREB model without correction terms relative to observed.



Figure 5

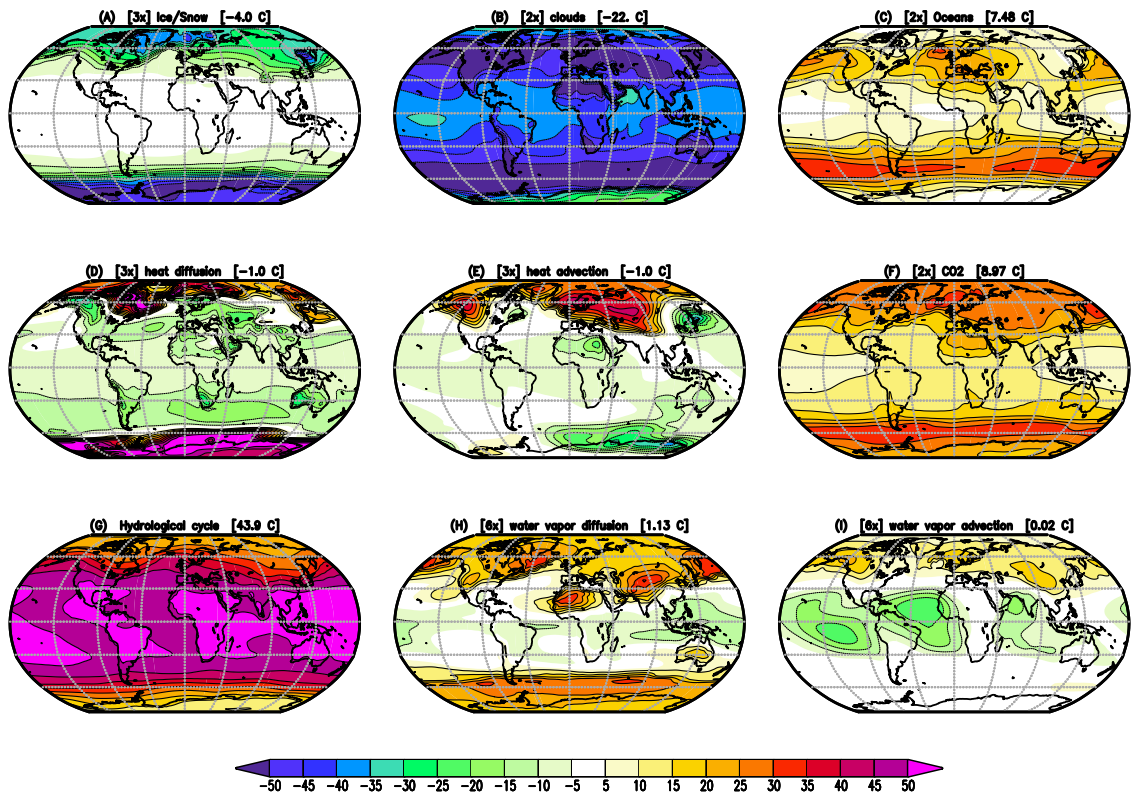


Figure 5: Changes in the annual mean T_{surf} in the GREB model simulations with different processes turned OFF as described in section 2a relative to the complete GREB model without model correction terms: (a) Ice/Snow, (b) clouds, (c) oceans, (d) heat advection, (e) heat diffusion, (f) CO_2 concentration, (g) hydrological cycle, (h) diffusion of water vapour and (i) advection of water vapour. Global mean differences are shown in the headings. Differences are for the control minus the sensitivity experiment (positive indicates the control experiment is warmer). All values are in $^{\circ}\text{C}$. In some panels, the values are scaled for better comparison: (b), (c) and (f) by a factor of 2, (a), (d) and (e) by a factor of 3, and (h) and (i) by a factor of 6.



Figure 6

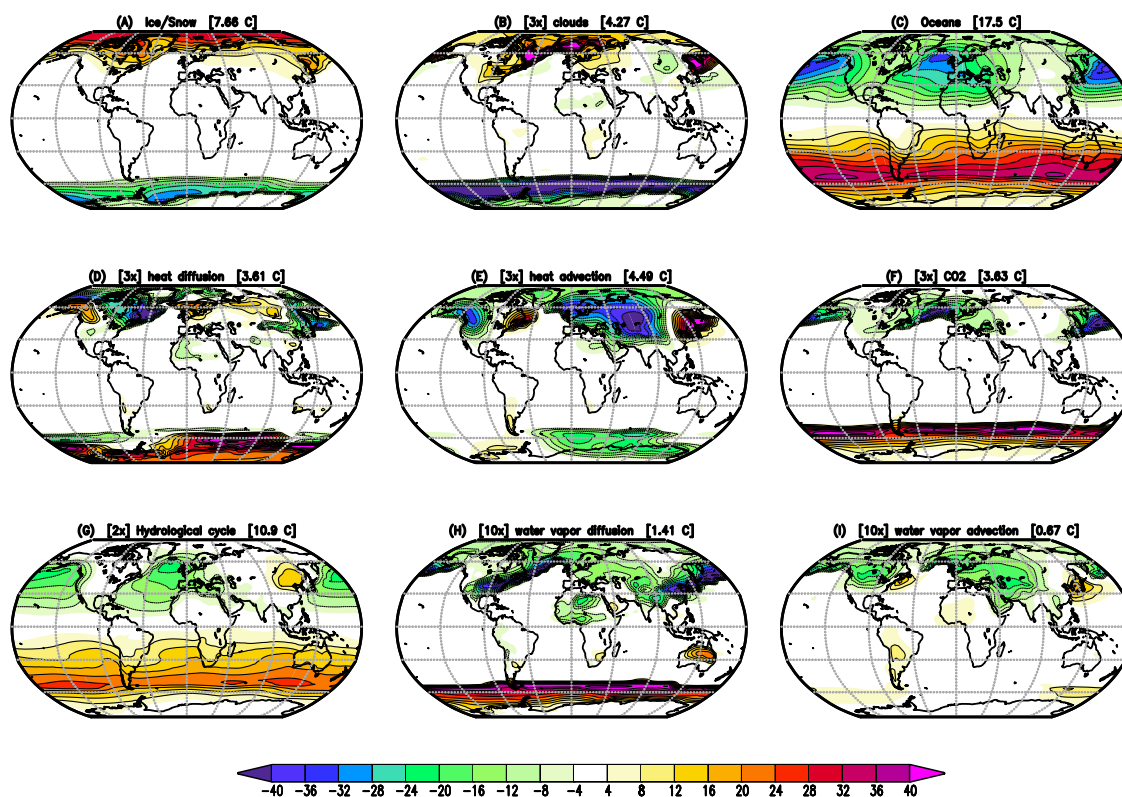


Figure 6: As in Fig. 5, but for the seasonal cycle. The mean seasonal cycle is defined by the difference between the month [JAS] - [JFM] divided by two. Positive values on the North hemisphere indicate stronger seasonal cycle in the sensitivity experiments than in the full GREB model. Vice versa for the Southern Hemisphere. Global root mean square differences are shown in the headings. All values are in $^{\circ}C$. In some panels, the values are scaled for better comparison: (b), (d) and (e) by a factor of 2, and (h) and (i) by a factor of 10. (g) is the mean for the hydrological cycle experiments with and without the ice-albedo process active.



Figure 7

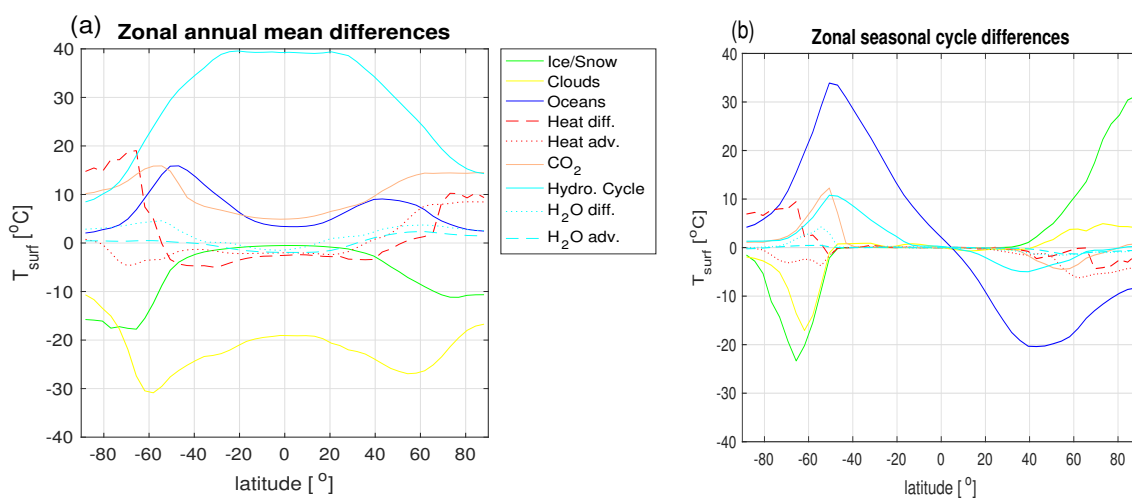


Figure 7: Zonal mean values of the annual mean (a) and seasonal cycle differences (b) for the experiments as shown in Figs. 5 and 6. g) The mean for the hydrological cycle is for the experiments with and without the ice-albedo process active.



Figure 8 part 1

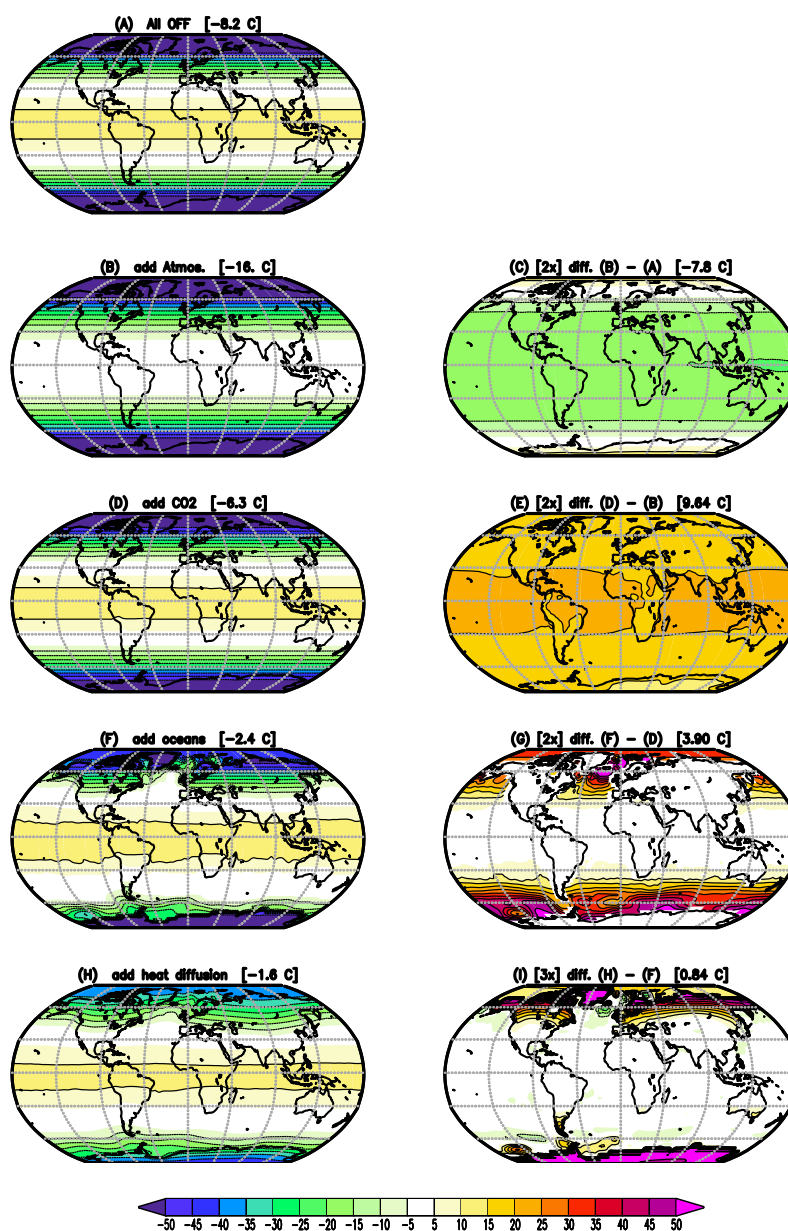


Figure 8: Conceptual build-up of the annual mean climate: starting with all processes turned OFF (a) and then adding more processes in each row: (b) atmosphere, (d) CO₂, (f) oceans, (h) heat diffusion, (j) heat advection, (l) ice-albedo, (n) hydrological cycle, (p) clouds and (r) water vapour transport. The panels on the right column show the difference of the left panel to the previous row left panel. Global mean values are shown in the heading. All values are in °C. In some panels in the right column the values are scaled for better comparison: (e), (g) and (q) by a factor of 2, (i) and (m) by a factor of 3 and (c), (k) and (s) by a factor of 4. For details see on the experiments see section 2a.



Figure 8 part 2

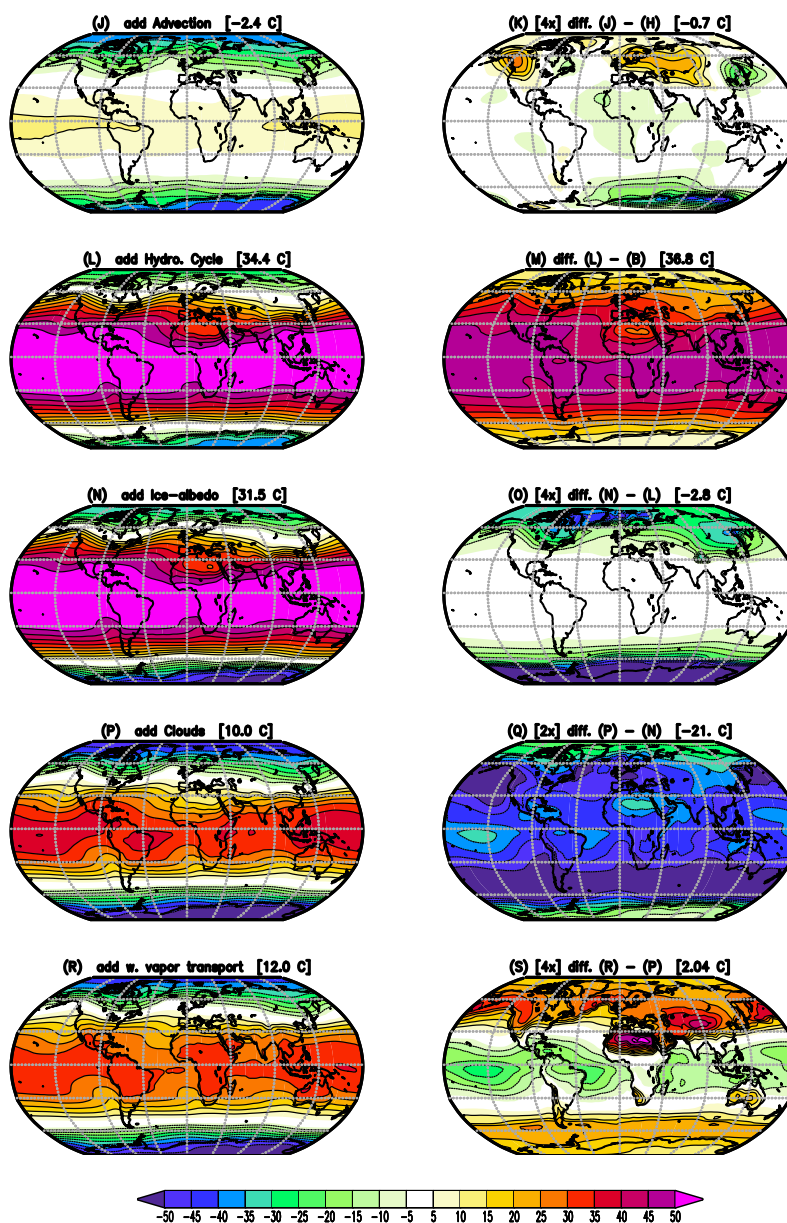




Figure 9 part 1

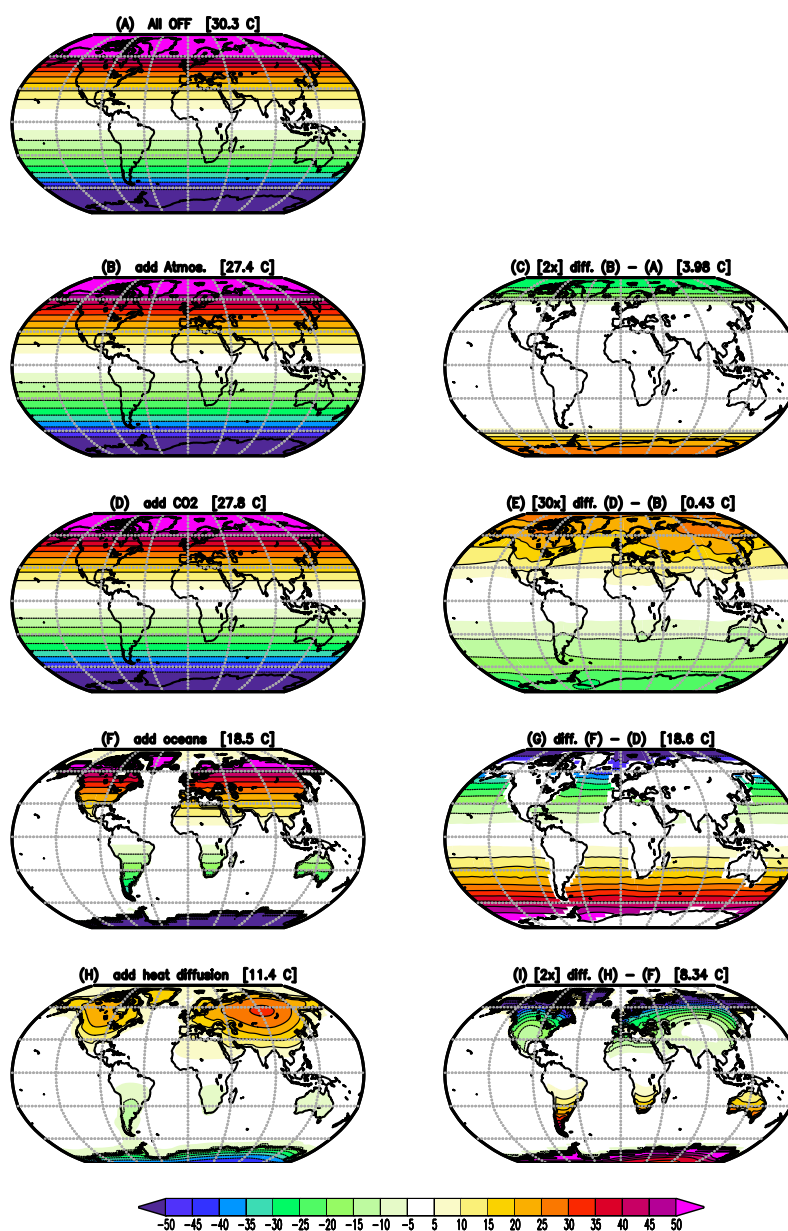


Figure 9: As in Fig. 8, but conceptual build-up of the seasonal cycle. The seasonal cycle is defined by the difference between the month [JAS] - [JFM] divided by two. Global mean absolute values are shown in the heading. In some panels in the right column the values are scaled for better comparison: (c) and (o) by a factor of 2, (i), (k), (q) and (s) by a factor of 5 and for (e) by a factor of 30.



Figure 9 part 2

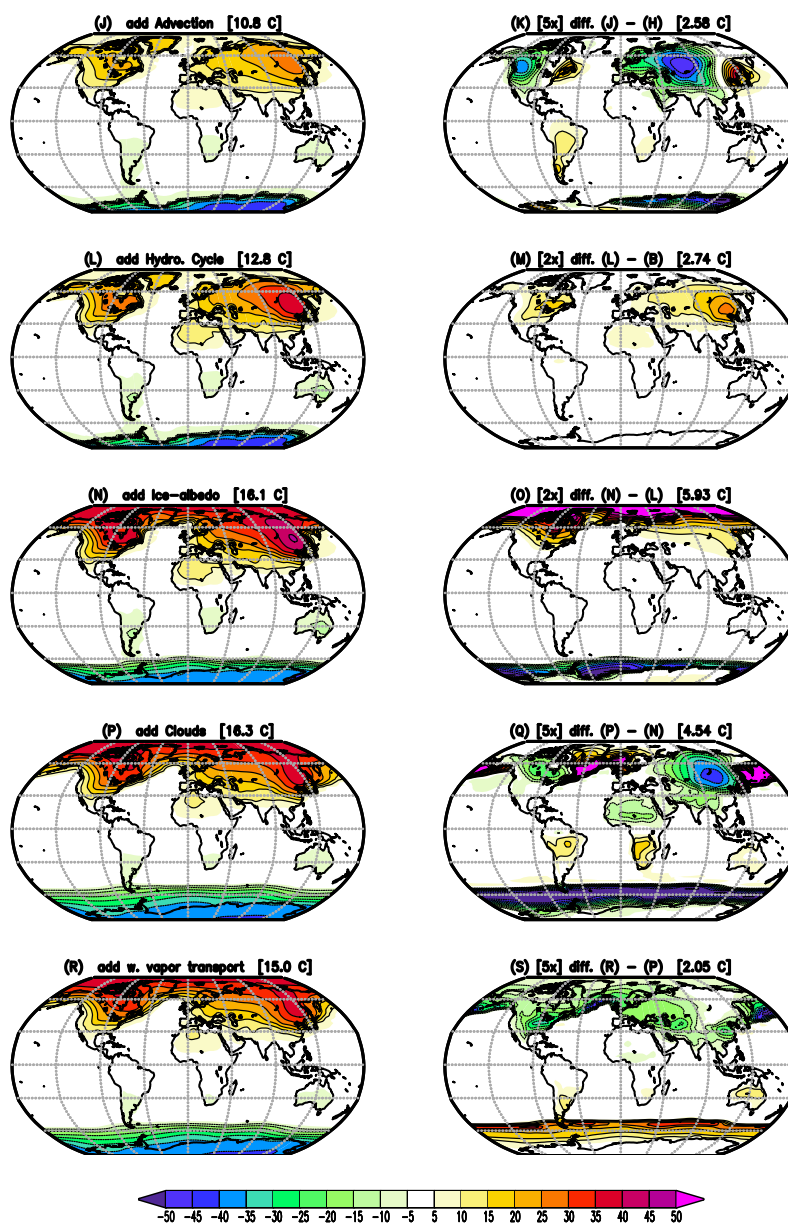




Figure10

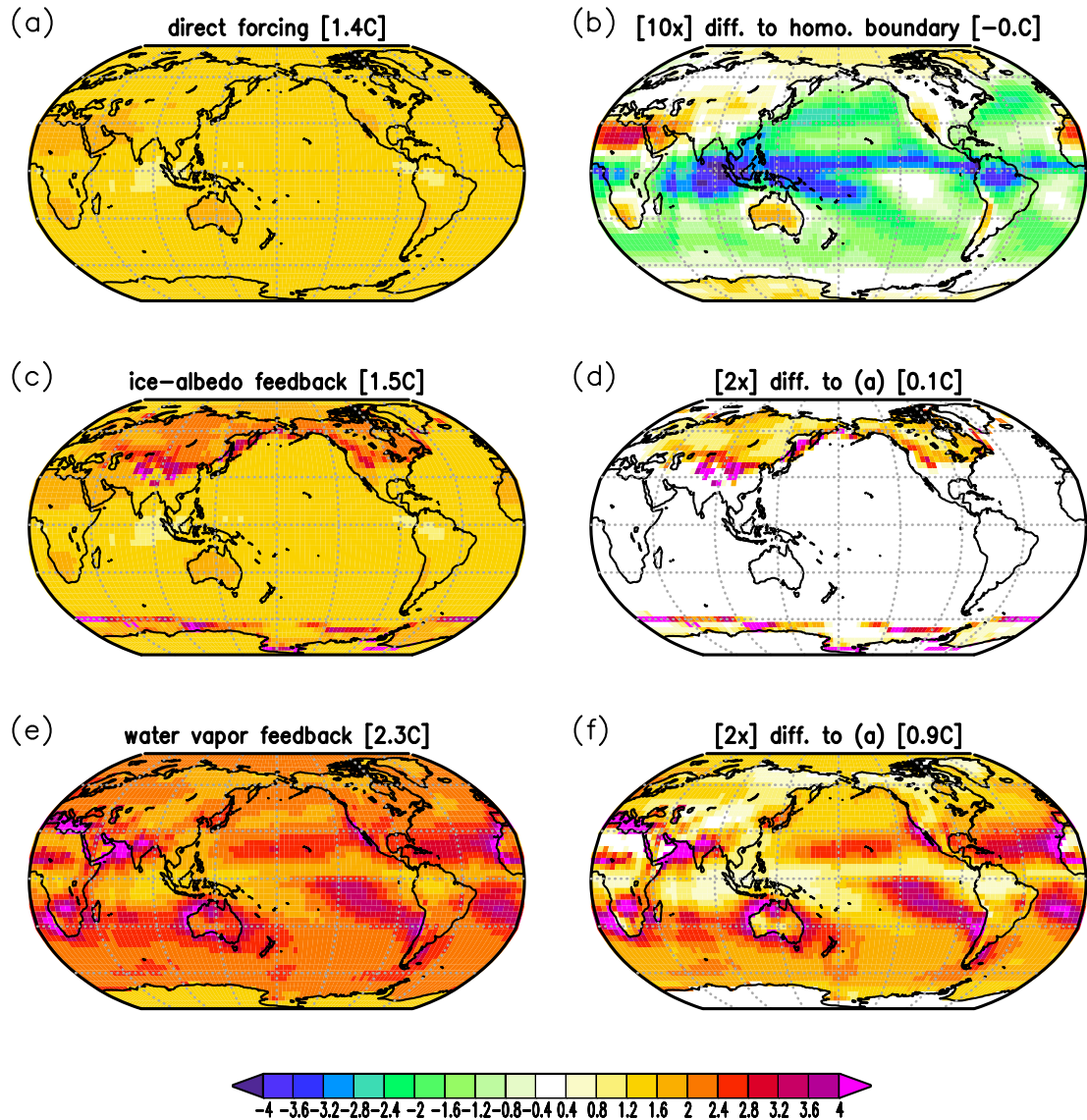


Figure 10: Local T_{surf} response to doubling of the CO_2 concentration in experiments without atmospheric transport (each point on the maps is independent of the others). (a) GREB with topography, humidity and cloud processes and all other processes OFF. (b) difference of (a) to GREB with topography and all other processes OFF scaled by a factor of 10. (c) GREB model as in (a), but with ice-albedo process ON. (d) difference of (c)-(a) scaled by a factor of 2. (e) GREB model as in (a), but with hydrological cycle process ON. (f) difference of (e)-(a) scaled by a factor of 2. For details see on the experiments see section 2b.



Figure 11

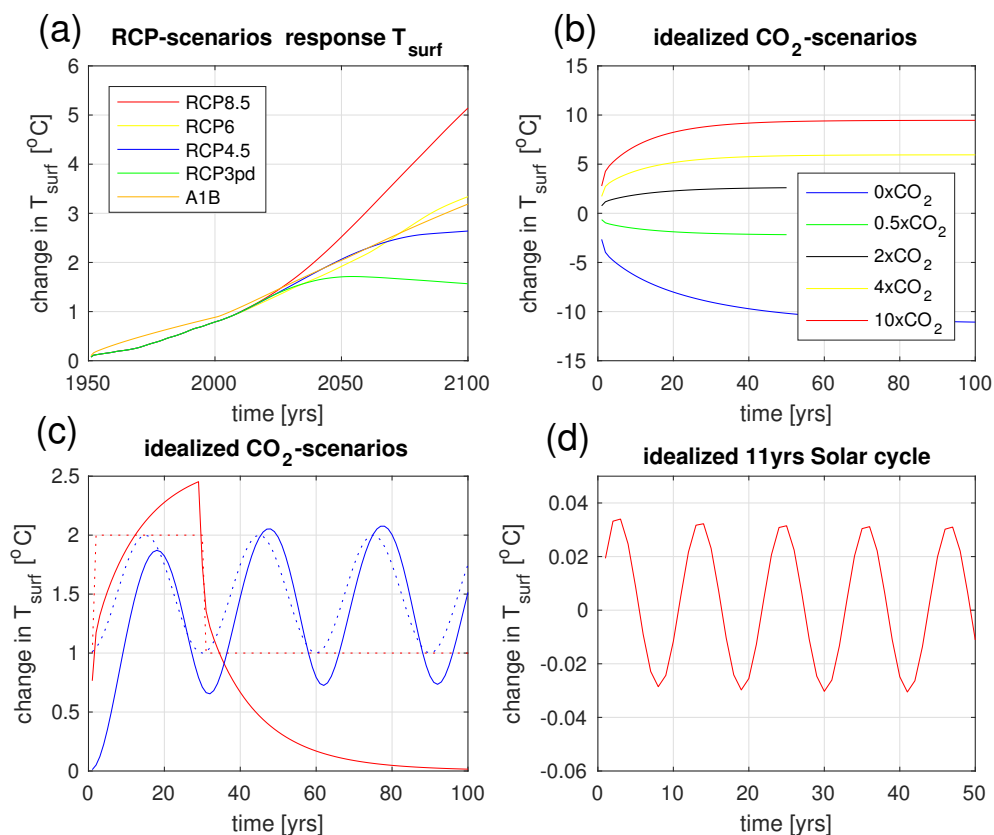


Figure 11: Global mean T_{surf} response to idealized forcing scenarios: (a) different RCP CO_2 forcing scenarios. (b) Scaled CO_2 concentrations. (c) idealized CO_2 concentration time evolutions (dotted lines) and the respective T_{surf} responses (solid lines of the same colour). (d) idealized 11yrs solar cycle. List of experiments is given in Table 3.



Figure 12

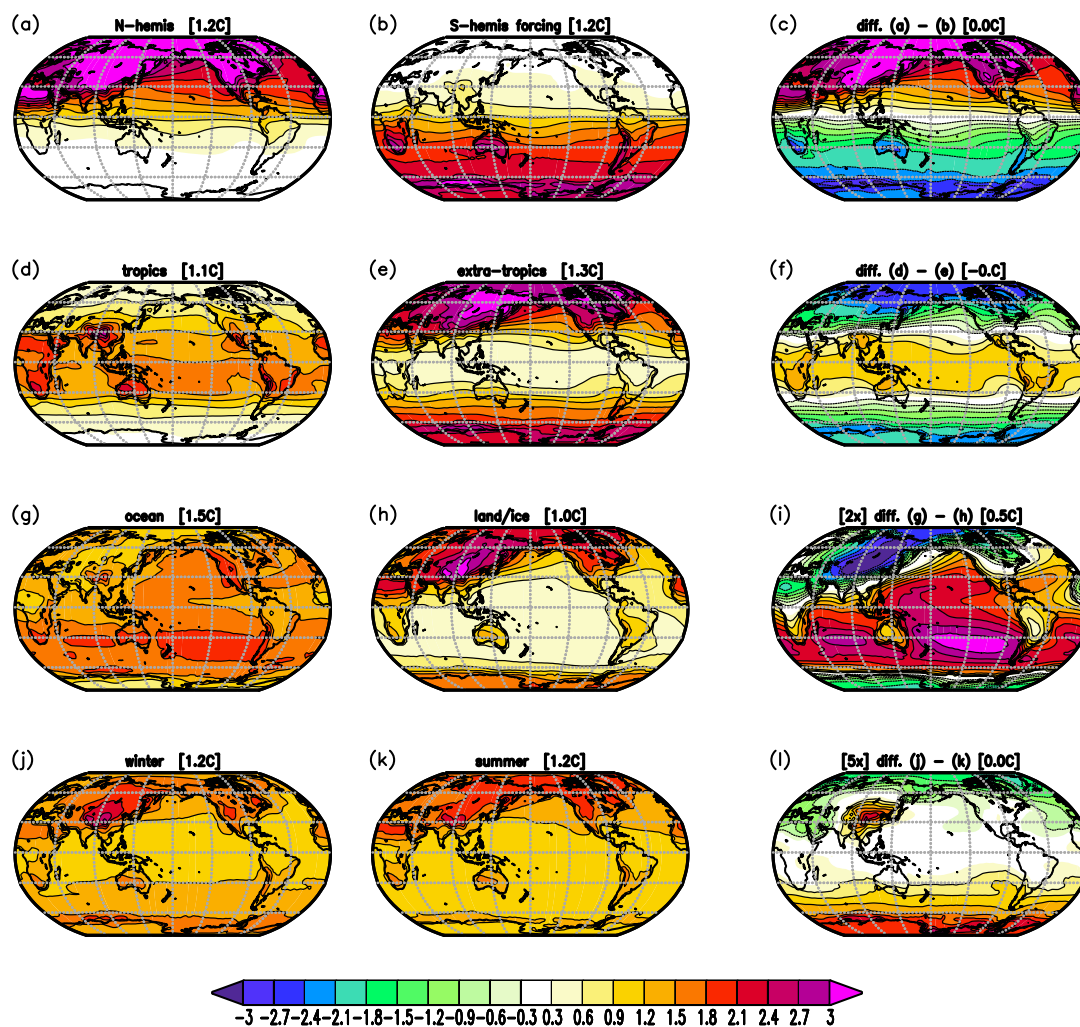


Figure 12: Tsurf response to partial doubling of the CO₂ concentration in: Northern (a) and Southern (b) hemisphere, tropics (d) and extra-tropics (e), oceans (g) and land (h), and in boreal winter (j) and summer (k). The right column panels show the difference between the two panels two the left in the same row.



Figure 13

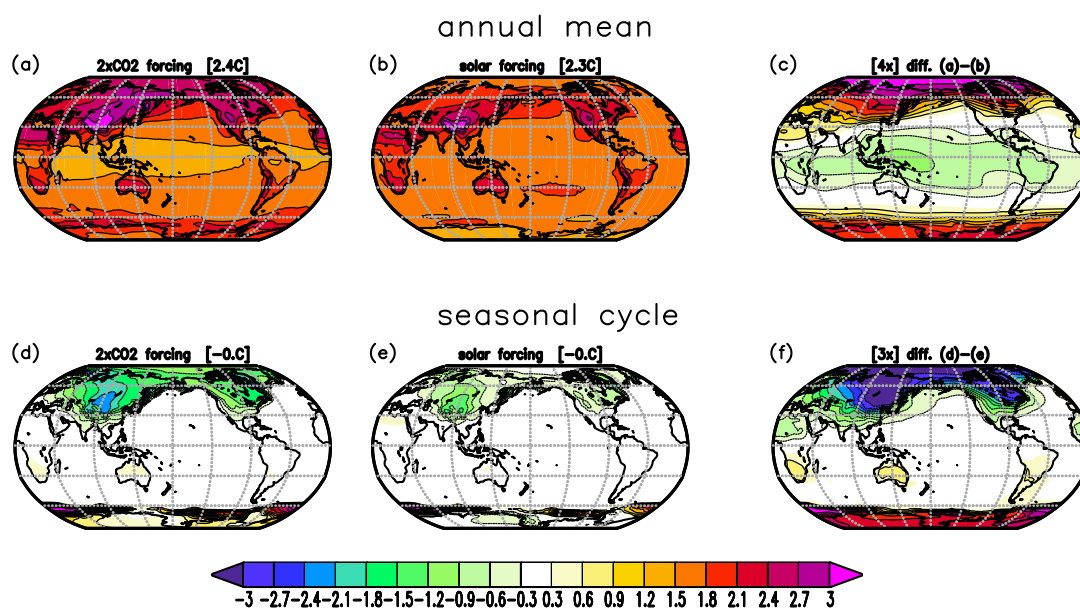


Figure 13: T_{surf} response to changes in the solar constant by $+27W/m^2$ (middle column) versus a doubling of the CO_2 concentration (left column) for the annual mean (upper) and the seasonal cycle (lower). The seasonal cycle is defined by the difference between the month [JAS] - [JFM] divided by two. The right column panels show the difference between the two panels two the left in the same row scaled by 4 (c) and 3 (f).



Figure 14

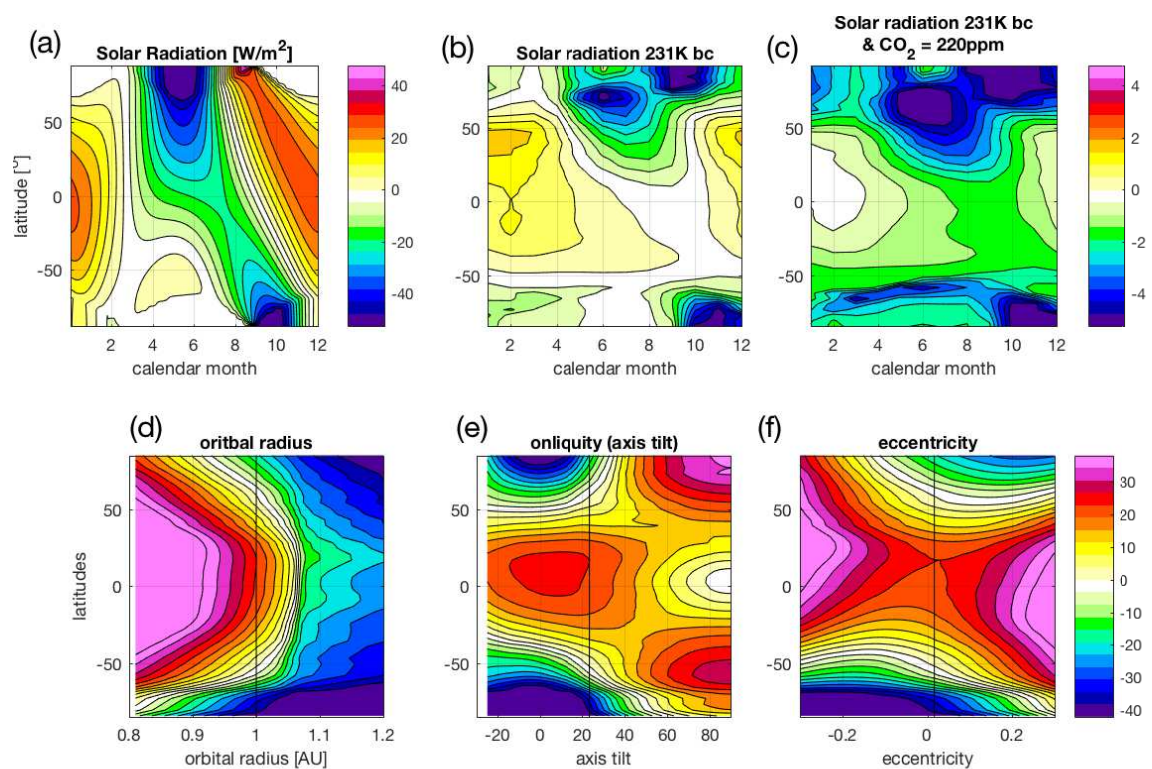


Figure 14: Orbital parameter forcings and T_{surf} responses: (a) incoming solar radiation changes in the Solar-231Kyr experiment relative to the control GREB model. T_{surf} response in Solar-231Kyr (b) and Solar-231Kyr-200ppm (c) relative to the control GREB model. Annual mean T_{surf} in Orbit-radius (d), Obliquity (e) and Eccentricity (f). The solid vertical line in (d)-(f) marks the control (today) GREB model.